University of Alberta

A molecular dynamics simulation study on the deformation behavior for nanotwinned polycrystalline copper

by

Arina Marchenko

A thesis submitted to the Faculty of Graduate Studies and Research
in partial fulfillment of the requirements for the degree of

Master of Science
in
Materials Engineering

Department of Chemical and Materials Engineering

Spring 2012
Edmonton, Alberta

Abstract

Present research is focused on the mechanical behavior of nanoscale copper with growth twins. Atomistic calculation (Molecular Dynamics simulation) with embedded-atom method potential was used to study the fundamental deformation processes that occur in columnar nanocrystalline copper. The research also investigates the influences of twin spacing and grain size on the deformation characteristics and properties of materials. Simulation results have shown that a material's strength and toughness can be enhanced by introducing twin boundaries within nanocrystalline grains. Nanotwins act as obstacles to dislocation motion that leads to the strengthening of nanotwinned structures, as well as sources of dislocation nucleation contributing to the toughness of the materials. The enhancement of the properties is more pronounced when the twin boundaries are close enough to the grain boundaries. At extremely small distance, the strength of the nanotwinned models is found to exhibit an inverse relationship. The deformation behavior in different grains depends upon their orientation with respect to the loading direction. The study has also revealed that grain-size refinement in nanotwinned models may deteriorate materials properties.

Acknowledgements

I am very grateful to a number of people for their contributions to this thesis. First, I would like to thank my supervisor, Dr. Hao Zhang for his excellent guidance and valuable advices through my entire study. I am also grateful for his patience and constructive criticisms that allowed me to complete this research without too much difficulty.

I owe a great deal of appreciation to my family that continuously supported me for the past two years in a numerous ways. In particular, this research will not be possible without my father's participation, who is, from my point of view, a genius in the area of programming. His exceptional knowledge and permanent guidance played one of the most important roles in the accomplishment of this study.

I also gratefully acknowledge all of my colleagues and friends that were always reliable and helpful to me. Special thanks to Elia Bastida, Artem Onyanov, Wenbo Xie, Alfonso Garcia, Yevgeniy Zagaevskiy for their encouragements and all moments that we shared together.

Table of Contents

List of Tables

List of Figures

Chapter 1. Introduction

Nanotechnology becomes the primary subject of research and the most growing area in science to date. Scientists throughout the world have recognized the potential importance of the nanotechnology field. The emerging applications in chemical, engineering, medical, optical, and electrical areas enable the continuing expansion of nanoscience in daily life [1]. The nanoscale dimension of the materials (typically less than 100 nm) leads to very different mechanical properties that are often exceptional and superior.

The combination of both high mechanical strength and high electrical conductivity is crucial for the conducting metals. Conventional methods to strengthen materials include grain refinement, solid solution alloying, second phase strengthening, dispersion strengthening and work hardening. All these approaches aim at introduction of internal defects that disrupt and impede the dislocation slip responsible for the occurrence of plastic deformation. Such strategies usually compromise the ductility and electrical conductivity of the material.

Nanocrystalline (NC) copper could be a candidate for the electrical contacts in dynamic systems due to its considerably improved mechanical strength [2]. Compared to its microcrystalline counterpart, nanocrystalline copper possesses considerably enhanced wear resistance. However, nanocrystalline Cu also suffers from undesirable conductivity impairment. Strong scattering of conducting electrons at high angle grain boundaries (GBs) promotes significant electrical resistivity of the metal. Recent investigations [3, 4] suggest that the

introduction of twin boundaries (TBs) can obtain materials with superior mechanical and electrical properties. Acting as conventional GBs, TBs are able to block the dislocation glide and thus provide substantial strengthening to the material [5]. At the same time, the electrical resistivity of the coherent internal TBs is about one order of magnitude lower than that of high-angle GBs [6]. As a result, nanotwinning is a novel approach to optimize mechanical performance of the material without compromising its high electrical conductivity.

Strength and ductility are the principal mechanical properties of any material but are also opposing characteristics due to the physical nature of plastic deformation. Nanotwinned structures are receiving a great deal of attention from researchers because they exhibit simultaneous improvement in strength and ductility with decreasing twin spacing [7, 8]. Significantly improved tensile ductility of nanotwinned materials is usually attributed to their pronounced ability to accommodate plastic strains before failure due to the interaction with interfacial dislocations while losing coherency [9].

Twinned structures are commonly observed in both coarse-grained and nanocrystalline materials. Conventionally, twin structure in bulk materials can be formed by various approaches such as plastic deformation, phase transformation, thermal annealing, and other physical or chemical processes [3]. Stacking fault energy defines the twinning tendency of a face-centered cubic (FCC) metals and alloys. Coarse-grained FCC [10] metals with high stacking fault energies such as Al and Ni normally deform by dislocation slip, while FCC metals with low stacking fault energy such as Ag primarily deform by twinning [10, 11]. The high

strain rate and low deformation temperature conditions also promote deformation twinning [12]. NC materials have a very different behavior in deformation twinning due to their small size. Deformation twinning in nanocrystalline metals will be discusses in details in the section 1.4.

Significant progress has been made in understanding the deformation twins in the last decade. Experimental evaluations [13] of NC copper with a focus on its mechanical properties are usually challenging since it is difficult to systematically investigate the local response of twin boundaries to stress at nanoscale. In this regard, atomistic simulation has been a useful and powerful tool for studying the deformation behavior of nanotwinned structures under the application of the external load [9, 14]. A comprehensive review of the experimental and computational studies of nanotwinned copper, its underlying deformation mechanism and the effect of various parameters, including the twin width and grain size, will be given in the literature review part of the present chapter.

The thesis consists of 4 chapters and is organized in the following way. Chapter 1 includes the motivation of the research and literature review dedicated to the nanocrystalline materials and twinned structures. Moreover, it gives the overview of the twinning processes in FCC metals, experiments and simulations related to nano-twinned structures and their mechanical properties. Chapter 2 outlines the fundamentals of the molecular dynamics method and the specific details of our simulation model setup. Chapter 3 presents the results obtained from the simulations. This chapter discusses the observed deformation behaviors, and

the stress-strain response of various nanotwinned models, the effects of twin width, and grain size on deformation behavior. The last chapter presents the summary of the studies and concluding remarks based on the results of the simulations, as well as recommendations for future work.

1.1. Nanocrystalline metals: mechanical properties

1.1.1. Yield strength

NC structures behave differently from their coarse-grained counterparts due to the scale dependency. The understanding of the influence of the grain size on the mechanical properties of nanocrystalline materials is the central question of the present section.

It is known that polycrystalline materials show a strong effect of grain size on hardness and strength. According to dislocation theory, the GBs act as obstacles to the dislocation slip causing dislocations to pile up on their slip planes behind the boundaries and to produce a stress concentration in the grain next to that containing a pile-up. By decreasing the grain size, we generate a high number of the GBs; however, the number of dislocations in the pile up decreases. As such, much larger applied stress is needed to cause slip to pass across the boundary in the fine-grained materials than in the case with coarse-grained materials. The higher the applied stress to move the dislocation, the higher is the yield strength. Thus, there exists an inverse relationship between grain size d and yield strength σ_y, which was originally proposed by Hall and Petch, and is known as the Hall-Petch equation:

$$\sigma_y = \sigma_0 + kd^{-1/2} \qquad [1.1.1.1]$$

where σ_0 is the friction stress below which dislocations will not move in a single crystal, and *k* is a Hall-Petch slope.

Once grain size falls down to a value below 10~20nm, there exists a limiting effect on the Hall-Petch behavior. This phenomenon is called the inverse Hall-Petch relation. The mechanisms that explain this unique behavior of materials are still controversial; however, several mechanisms have been proposed to explain it. The first clear inverse Hall-Petch behavior for nanostructured materials was observed by Chokshi et al [15] for nanocrystalline Cu and Pd for grain size less than 16 and 14 nm respectively. The authors explained it by the occurrence of rapid diffusion creep at room temperature, i.e. coble creep was considered as the deformation mechanism. The deviation from the Hall-Petch relation can be also explained by the dislocation theory: once grain size drops below the equilibrium distance between dislocations, the pile up of dislocations against the grain boundaries is insignificant. As a result, the Hall-Petch relationship is no longer valid, and the conventional dislocation activity ceases. Furthermore, GBs in NC materials occupy a larger fraction of the volume than that in coarse-grained. As such, grain boundary contributions to the deformation become dominant, and can also cause the departure from the classical Hall-Petch relation. MD simulations performed for FCC metals by Van Swygenhoven [16] indicate that at the critical grain size, all plastic deformation is accommodated in the GB and the decrease in yield strength is attributed to the GB sliding. Yamakov et al. [17] proposed a deformation-mechanism map for the mechanical behavior of

nanocrystalline FCC metals that captures the transition in the deformation mechanisms and the related mechanical behavior with decreasing grain size. Some deformation mechanisms contributing to the plasticity at nanoscale include partial dislocation emission from GBs [10][18], transmission across the NC grain, and absorption into the opposing GBs. Mechanical twinning at relatively higher strain rates and stresses, reported by Yamakov et al. for 2-D columnar Al [19, 20] also plays an important role in the deformation behavior of nanocrystalline materials. The softening can also be attributed to the presence of voids and unrecognized pores in the sample, as well as poor sample quality.

1.1.2 Ductility

Ductility of NC materials, defined as the ability of a material to deform under tensile stress without breaking, is poor compared to coarse-grained counterparts with the percentage elongation below 10%. Figure 1.1 illustrated elongation to failure in tension plotted versus grain size for a variety of metals and alloys. It is clear from the plot that for most metals with grain sizes below 30 nm the elongation to failure values are very low, typically less than 2-3%. Koch et al. [21] has identified three major sources of such an early fracture: (1) artifacts from processing such as pores inside the samples that trigger failure sometimes before yielding starts; (2) tensile instability or a concentration of large deformation in one region that results in a crack formation and an early failure or necking in tension; (3) crack nucleation or shear instability.

In addition, due to their size, NC grains fail to efficiently store the dislocations, leading to the low ductility of materials [4].

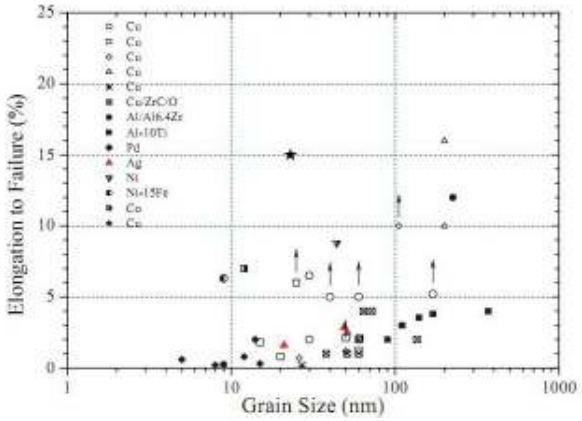

Figure 1. 1 Elongation to failure in tensions vs. grain size for a variety of metals and alloys [22].

In order to obtain both high strength and good ductility in NC materials, the processing flaws have to be minimized or eliminated. The various methods for producing materials with the minimum processing artifacts are known: vapor-deposition processes (sputtering, electron beam evaporation, pulse laser ablation can provide essential artifact-free NC materials to the finest grain sizes); electrodeposition with no additives; crystallization of amorphous precursors etc. Furthermore, the introduction of special twin boundaries in nanocrystalline structures has been proposed as one mechanism to enhance ductility [23]. The effect of these boundaries will be discussed further in section 1.3.

1.1.3 Strain hardening

Strain hardening occurs mostly for ductile materials. It is usually observed in the plastic region with a high lattice dislocation accumulation. In the case of NC, strain hardening is limited at grain sizes where dislocation activity is believed to be difficult. The dislocations traversing the small grains in order to sustain the

plastic flow tend to annihilate into the opposing GBs, preventing the accumulation of large strains in the local regions and leading to the low rate of strain hardening [4]. In this regard, GBs act both as the source of dislocation generation and their sinks in NC grains.

An approach that has been used to provide strain hardening in nanocrystalline materials is to introduce a bi-modal grain-size distribution by appropriate processing methods [2, 24-26]. Twin boundaries can also be an effective obstacle to dislocation motion and a potent strengthener. The further discussion of TBs effect will be provided below.

1.2 Deformation mechanisms in nanostructured materials

The unique mechanical properties of NC are controlled by their deformation mechanisms. Several deformation mechanisms have been identified in NC materials: GB sliding, grain rotation, partial dislocation emission from GBs and deformation twinning. The significance of each deformation mechanism changes with decreasing grain size. The key deformation processes and tendencies at the nanoscale level are discussed in this section.

1.2.1 Grain boundary sliding

GB sliding represents the relative slide of the layers of neighboring grains that produces a shear strain during the process. Figure 1.2 illustrates a schematic process of the sliding.

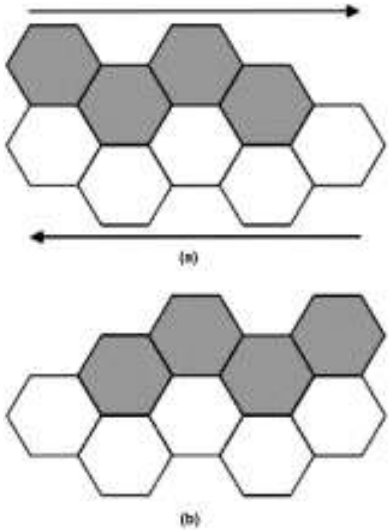

Figure 1. 2 Grain boundary sliding model: (a) initial position of grains and (b) position after top layer has slid to right [27].

First GB sliding was observed in NC materials in MD simulations [17, 18, 28, 29], and later reported in experiments [30, 30-32]. At the micro scale, GB sliding occurs either by movement of GB dislocations or by local shear events. The first mechanism includes the movement of GB dislocation glide with Burgers vector parallel with the corresponding boundary planes [33]. The movement of the GB dislocation is driven by the shear stress and carries plastic flow localized in the dislocation cores [1]. An alternative mechanism represents GB sliding as the thermally activated local shear events which include either individual atomic jumps or local transformations of small groups of atoms in the GB phase [28, 34]. Conrad et al.[35] suggested that GB sliding results from the combined action of thermally activated local shear events, and proposed a formula for the corresponding macroscopic plastic shear rate γ:

$$\frac{d\gamma}{dt} = \left(\frac{6av_D}{d}\right)\sinh\left(\frac{v\tau_e}{kT}\right)exp\left[-\frac{\Delta F}{kT}\right] \qquad [1.2.1.1]$$

where a denotes the mean interatomic distance in the GB phase, d is the grain size, v_D is the Debye frequency, k is the Boltzmann constant, T is the absolute temperature, τ_e is the effective shear stress, ΔF is the Helmholtz free energy. Formula [1.2.1.1] establishes the dependence of the yield stress on grain size in the case where GB sliding is the dominant deformation mechanism. Particularly, it explains the inverse Hall-Petch relationship in NC materials where the dependence shows a decrease of the yield stress with reducing grain size.

1.2.2 Grain rotation

The experimental observation [36] and computational confirmation [37, 38] of grain rotation during the plastic deformation of NC materials point out that the grain rotation plays a significant role in the deformation of metals and alloys. Rotational deformation can occur via the motion of GB-disclinations [39] that represent line defects of the crystalline lattice separating GBs with different misorientation parameters. Movement of a dipole of disclinations, which is a combination of two disclinations, carries plastic flow accompanied by crystal lattice rotation behind the disclinations. Alternatively to the disclination motion, Ma and coworkers [40-42] suggested that rotated nanosized grains could also coalesce along directions of shear, creating larger paths for dislocation movement. Figure 1.3 shows this in schematic fashion.

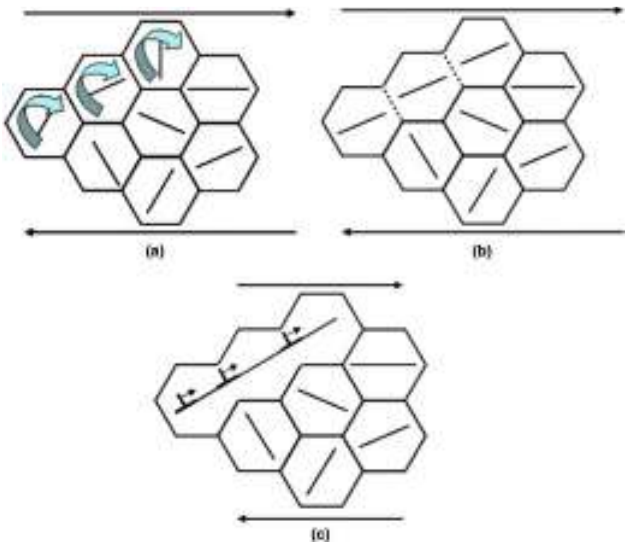

Figure 1. 3 Rotation of neighboring nanograins during plastic deformation and creation of elongated grains by annihilation of grain boundary [27].

The orientations of the slip systems with highest Schmid factors are represented by a short line in each grain (Figure 1.3(a)). As plastic deformation takes place, two neighboring grains might rotate in a fashion that brings their orientation closer together (Figure 1.3 (b)). This leads to the elimination of the barrier presented by the boundary between them, providing a path for more extended dislocation motion (Figure 1.3 (c)). This mechanism can lead to softening and localization, and is consistent with the limited ductility often exhibited by nanocrystalline metals.

1.2.3 Dislocation emission from GBs

It is known that the plastic deformation of coarse-grained FCC metals involves generation of multiple dislocations from Frank–Read sources and their glide motion through the crystal [43]. With a decrease of the grain down to nanometer scale, GBs become the dominant dislocation sources and sinks. This

phenomenon was reported in the papers dealing with experimental studies [44, 45] and MD simulations [43, 46, 47] of plastic deformation in nanostructured materials. For the NC materials that are characterized by large volume fraction of the GB phase, GBs play a dual source-sink role of perfect and partial lattice dislocations. Partial dislocations, usually called Shockley partials, have a Burgers vector of 1/6 [112] and are connected by a stacking fault. Their splitting distance between two partial dislocations depends on the stacking-fault energy and the applied stress [48].

The simulations of columnar nanostructured Al [43] show the emission of partial and split distance dislocations from the GBs. It was revealed that the dislocation regime depends on grain size d and splitting distance r_{split}, described with the formula

$$r_{split} = \frac{Kb^2}{\gamma - b_p m\sigma} \qquad [1.2.3.1]$$

where $b_p = a/\sqrt{6}$ denotes the Burgers vector magnitude characterizing a partial dislocation, a is the crystal lattice parameter, γ is the stacking fault energy density, m is the Schmid factor, K is a factor depending the elastic constants of the material, and σ is the external stress. When $r_{split}>d$, then a single partial dislocation is emitted from a GB, glides through the grain leaving behind the stacking fault, and eventually is absorbed by an opposite GB. If $r_{split}<d$, two Shockley partial dislocations are consequently emitted from a GB and form a split lattice dislocation that moves towards an opposite GB.

Plastic deformation of NC Cu [49] with grain sizes from 5 to 50 nm also show a shift in deformation mechanism, from dislocation-mediated plasticity at larger grain sizes to grain boundary sliding at smaller. The dislocation activity in the grains is dominated by the GBs, as almost all dislocation nucleation occurs at the grain boundaries, which also act as efficient dislocation sinks.

1.2.4 Summary of NC materials

The following mechanical properties of NC can be concluded. First, NC materials posses extremely high yield strength. In the range of small grain sizes (10 nm), the dependence of the yield stress on the grain size deviates from the classical Hall-Petch relations. Secondly, NC materials commonly tend to exhibit much reduced ductility due to processing flaws as well as low efficiency of the grains to store the dislocations, leading to an early necking in tension or failure. The above facts are defined by the unique deformation behavior of NC materials including extended partial and full dislocation emissions from the GBs, grain sliding and rotation.

1.3 Nanotwinned structures

Similar to conventional nanoscale GBs, twin boundaries (TBs) may also be an effective obstacle to dislocation motions and a potent strengthener. Nanotwinned structures, containing a high density of nano-scale twins within the grains, exhibit an unexpected improvement in both strength and ductility with decreasing twin spacing. The strength enhancement with twin refinement is comparable to that observed in nanocrystalline Cu samples due to grain refinement. Significant progress has been made in understanding the deformation

twins in the last decade. In the present section the following review is given: aspects of deformation twinning in NC metals and alloys, including deformation twins observed by MD simulations and experiments, the effects of deformation twinning on mechanical and electrical properties, mechanisms and factors affecting twinning fault formation.

1.3.1 Twin boundaries

Twin boundaries (TBs) represent special highly symmetrical low energy interfaces with one crystal the mirror image of the other across the coherent twin boundary plane. The atoms are shared by the two crystals at regular intervals. In FCC metal, the mirror symmetry can be viewed along the [1 1 0] orientation on the coherent twin plane (see Figure 1.4).

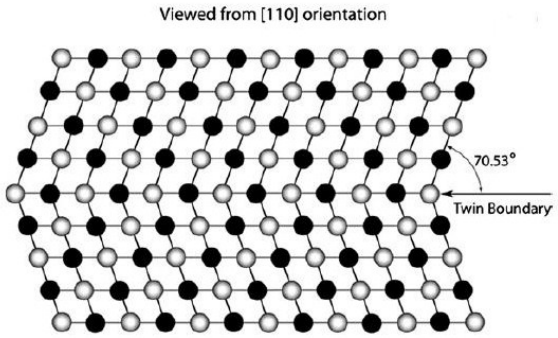

Figure 1. 4 The mirror symmetry of atoms in a twin in FCC metals, when viewed from a [1 1 0] direction that is on the coherent twin boundary plane [11].

As shown, the coherent twin boundary plane is the (111) close-packed plane and it has a 70.53^0 angle with other close packed planes. The mirror symmetry structure marked with the red line is shown in Figure 1.5 in the high-

resolution electron microscopy (HREM) image. TBs can be as effective an obstacle to dislocation movement as GBs. Thus, they are believed to contribute in the plastic deformation and strengthening of nanocrystalline materials.

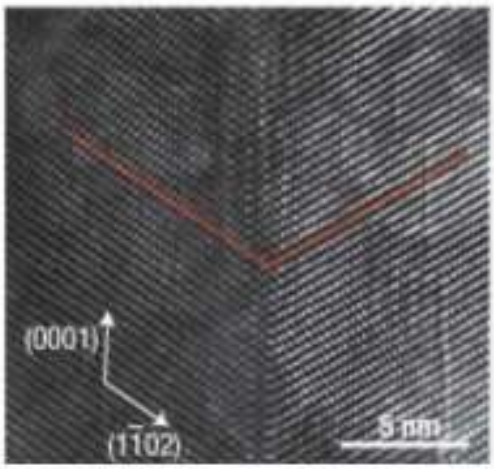

Figure 1. 5 High-resolution electron microscopy image of deformation twins in alumina fragments. The red lines show the mirror symmetry of the twin band with the matrix [50].

1.3.2 Mechanical properties of nanotwinned structures

Experimental observations and recent simulation results indicate that the introduction of the nano-scale twins within ultrafine crystalline metals leads to enhanced tensile strength and elevated hardness of the material. Strengthening effect by means of twins is attributed to the interaction between the TBs and dislocations. The presence of twins hinders free dislocation movement and causes dislocation pile-ups at the TBs. When the twin lamellae are thick, a large number of dislocations assemble together in the pile-up and produce a stress concentration at the TBs. Thus, less applied stress is required for slip transmission across the

TBs. However, for thin lamellae, only one or two dislocations may gather at the pile-up and hence, extremely high external stress is needed for dislocation transmission across the TBs. In this sense, the TBs behave more like the GBs in strengthening of materials at the nanoscale. The tensile stress-strain curves for polycrystalline Cu containing different volume fraction of nano-sized growth twins at various strain rates are shown in Figure 1.6.

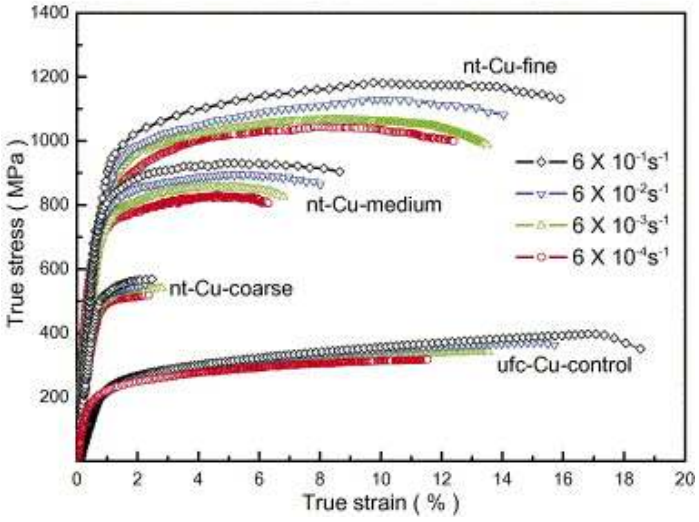

Figure 1. 6 Tensile stress-strain curves of as-deposited Cu with various twin densities tested at different strain rates [7].

As shown, yield strength and tensile strength increase with increasing loading rate. Furthermore, as the twin spacing decreases, the yield strength and, tensile strength increase. These trends, caused by the introduction of nanotwins, are comparable to those observed in nanocrystalline Cu samples due to the grain refinement. However, compared to the grain size reduction, the enhancement in strength with the introduction of nanoscale growth twins occurs without reduction

in ductility. Shen et al. [8] reported considerable increase in elongation-to-failure with decreasing TB density.

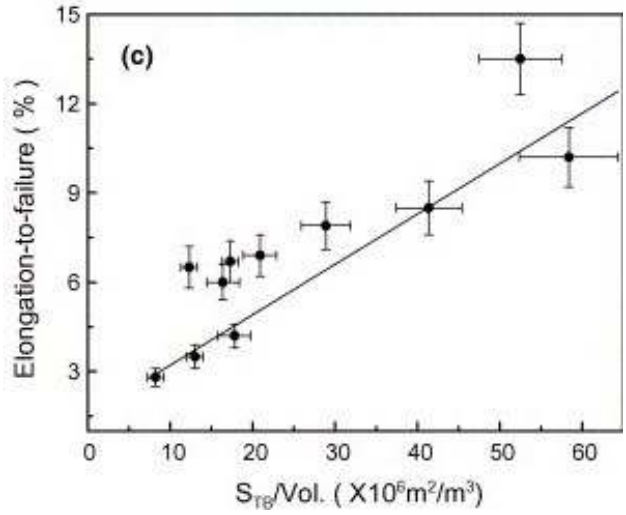

Figure 1. 7 Tensile elongation-to-failure vs. the twin lamella density from TEM observations of as-deposited Cu samples [8].

This enhanced ductility has also been reported to be caused by dislocation interactions with the TBs. It is known that when a dislocation crosses a TB a dislocation dissociation reaction takes place and a Shockley partial dislocation is left behind at the TB, which may accommodate plastic straining. Therefore, the higher the TB density, the larger the density of accumulated dislocations at the TB, which results in enhanced ductility due to plastic deformation.

1.3.3 Softening phenomena in nanotwinned Cu

Lu et al. [51] investigated the yield strength of nanotwinned Cu samples with the twin thickness ranging from 4 nm to 100 nm. The corresponding stress-strain curves are shown in Figure 1.8. The results demonstrated continuous

increase in strength while decreasing the thickness of twins down to 15 nm. However, further reducing the thickness resulted in softening accompanied by impaired strain hardening and tensile ductility. The observed softening behavior was attributed to the increased dislocation arrays at the GBs and preexisting dislocation density at the TBs, both of which can act as potential dislocation sources to initiate plastic deformation.

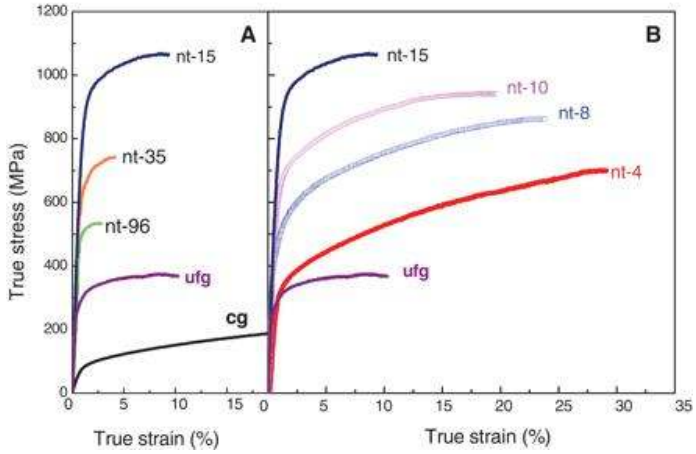

Figure 1. 8 Tensile true stress–strain curves of nanotwinned copper tested at a strain rate of $6x10^{-3}$ s^{-1}.(Curves for a twin-free ultrafine –grained Cu with a mean grain size of 500 nm and for a coarse-grained-Cu with a mean grain size of 10 mm are included for the comparison [51].

The maximum strength observed by Lu et al. [51] was further investigated using large-scale MD simulations and a kinetic theory of dislocation nucleation by Li et al. [52]. They proposed a dislocation–nucleation-controlled mechanism in nanotwinned metals, in which there are plenty of dislocation nucleation sites but dislocation motion is not confined. They showed that dislocation nucleation governs the strength of such materials, resulting in the softening of the materials

below a critical twin thickness. They found that there exists a transition in deformation mechanism occurring at a critical TB spacing for which strength is maximized. At this point, the classical Hall–Petch type of strengthening due to dislocation pile-up and cutting through twin planes switches to a dislocation–nucleation-controlled softening mechanism with twin-boundary migration resulting from nucleation and motion of partial dislocations parallel to the twin planes.

1.3.4 Electrical properties of nanotwinned structures

High electrical conductivity of nanotwinned Cu is another important property that makes nanotwinned Cu a good candidate for electrical contacts in dynamic systems. Due to ordered structure, the scattering of conducting electrons at the TBs is much less than that of GBs. According to Lu et al. [3], the electrical resistivity of nanotwinned Cu sample is much less than that of the NC Cu without twins, and very close to that of the coarse-grained Cu specimen over a wide temperature range, as shown in Figure 1.9. The total electrical resistivity of a crystal can be described as a sum of the resistivity due to thermal agitation of the metal ions, and the resistivity due to imperfections in the crystal such as dislocations and grain boundaries. The major factor that contributes to the difference in electrical resistivity is grain boundaries and twin boundaries, while the difference in the lattice dislocation density among the samples could be ignored. As the electrical resistivity of the coherent TBs is much smaller than that of GBs, the nanotwinned samples have conductivity that is close to that of the coarse-grained Cu.

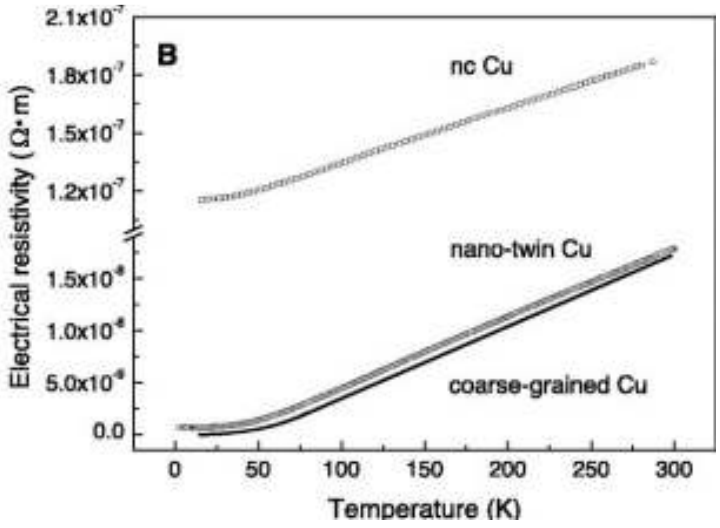

Figure 1. 9 Measured temperature dependence of electrical resistivity for the as-deposited nanotwinned Cu sample and the coarse-grained sample [3].

1.4 Deformation twinning in FCC metals

1.4.1 Generalized stacking fault curve

Similar to the slip process, deformation twinning is one of the modes of plastic deformation that usually occurs as the result of applied stresses. During this process, a region of a crystal undergoes a homogeneous shear that produces original crystal structure in a new orientation. The result of the deformation twinning is the formation of highly symmetrical interfaces TBs, one side of which contains arrangements of atoms that are mirror reflections of those on the other side separated by the twin composition plane [53].

The existence of deformation twinning in FCC materials has been ignored in dislocation dynamics studies until 1957, when Blewitt, Coltman and Redman [54] performed tensile tests on a single crystal of Cu at low temperatures 4.2 K and 77.3 K and observed mechanical twinning using X-ray method. Later

experimental studies have also reported additional observations of twinning in FCC materials [55, 56]. The transmission electron microscope observations of plastically deformed NC Al [57] confirmed the evidence of deformation twinning in NC materials. The experimental observations of deformation twins in NC materials were further validated by MD simulations [58, 59].

In FCC materials, stacking faults and deformation twins usually occur in metals and alloys with low stacking fault energy, although high strain rate and low deformation temperature can significantly promote twinning [11]. In the low stacking fault energy FCC metals, deformation twinning and dislocation slip can be considered as two competing processes. The generalized stacking fault (GSF) curve (Figure 1.10), that is also called the energy-displacement curve, shows the energy required to shift adjacent atomic planes past one another.

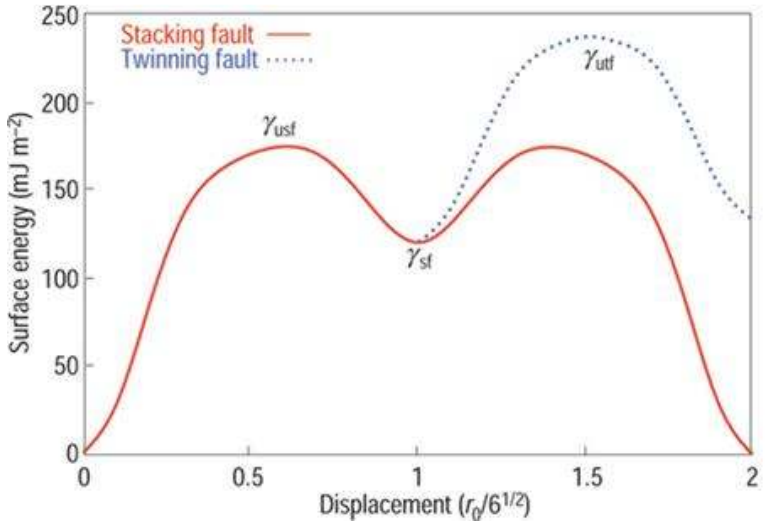

Figure 1. 10 Generalized planar fault curve showing unstable stacking fault γ_{usf}, stacking fault γ_{sf}, and unstable twinning fault γ_{utf} [10].

γ_{usf} denotes the unstable fault energy and represents the amount of energy required to nucleate a partial dislocation [10]. The propagation of the leading partial dislocation produces a stacking fault behind it [60] with stacking fault energy termed γ_{sf}. At this point two possible scenarios can occur: a trailing partial dislocation can emit at the same plane overcoming the energy difference (γ_{usf}-γ_{sf}) and leading to full dislocation slip; otherwise, a partial dislocation of the same Burgers vector can emit at the adjacent slip plane, forming a microtwin boundary [10]. According to Swygenhoven [10], both stable and unstable stacking fault energies should be taken into consideration for a better estimation of the nature of slip in NC metals. When the ration of $\frac{\gamma_{sf}}{\gamma_{usf}}$ approaches unity, the energy barrier that has to be overcome in order to create a trailing partial becomes low; therefore, full dislocation activities become possible. Otherwise, when the ratio is low, only the leading partial propagates through the grain forming an extended partial dislocation, which is the case for Ni and Cu. Similarly, for the second alternative path, the emission of a partial dislocation in the neighboring plane forming a deformation twin depends upon the ratio of $\frac{\gamma_{utf}}{\gamma_{usf}}$, where γ_{utf} is the unstable twinning fault [10, 61].

1.4.2 Mechanical twinning in nanocrystalline materials

Experimental observations and MD simulations results have revealed different twinning mechanisms in NC materials. Formation of deformation twins via emission of Shockley partials from GBs was first predicted by MD simulations [20] (Figure 1.11), and later verified by HREM (Figure 1.12). The

mechanical twinning processes in the deformation of a NC Al was described in a work of Yamakov et al. [62].

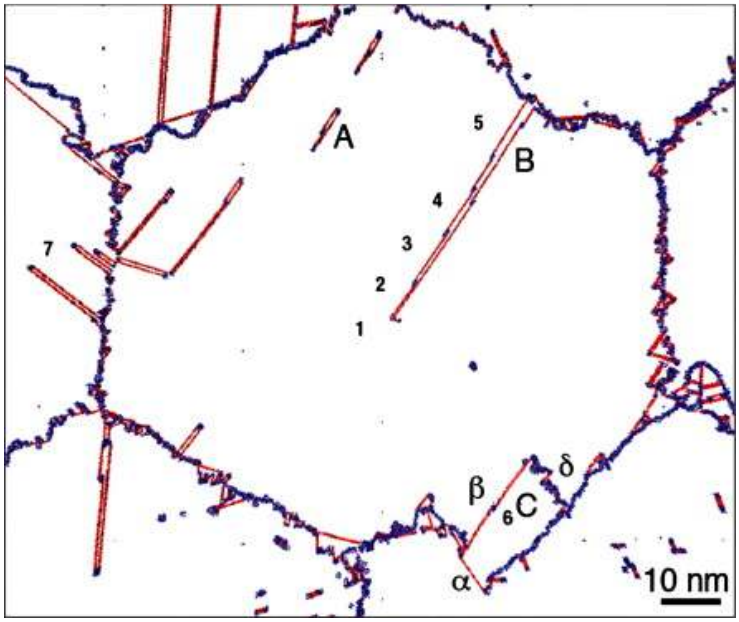

Figure 1. 11 Three twinning mechanisms are revealed in this MD simulation snapshot of nc Al with columnar grains [20].

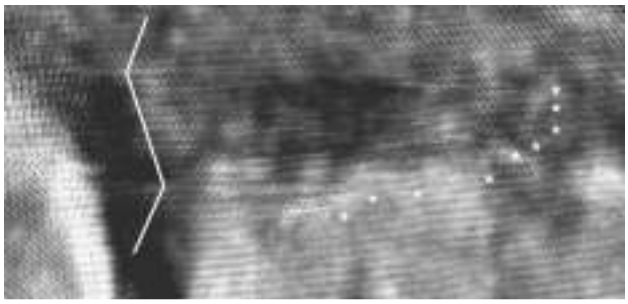

Figure 1. 12 An HREM image of a twin formed by plastically deforming electrodeposited NC Ni. The twin was formed by the emission of partials from the grain boundary on the left, and it ended in the grain interior as marked by the white asterisks [63].

From Figure 1.11 several processes of twin formation during the plastic deformation involving GBs (heterogeneous nucleation) and grain interior (homogeneous nucleation) could be seen [62]:

1) Region A: twin nucleus formed by the overlapping of two extended dislocations on adjacent slip planes;

2) Region B: twin formed by successive emission of five Shockley partials from the GB;

3) Region C: twin formed by splitting of a GB and subsequent migration, which leaves behind two coherent TBs (α, β), while the migrating TB (δ) consists of a Shockley partial dislocations;

These twins and twin faults reacted with dislocations and formed complex twin networks, including coherent twin boundaries.

1.4 Dislocation-twin boundary interaction in FCC metals

The simultaneous occurrence of deformation twinning and dislocation slip of perfect dislocations and partial dislocations in FCC metals promotes interactions between twins and gliding dislocations at TBs. Dislocation reactions at TBs are believed to be the reason of high strength and ductility of NC materials. Atomistic simulations conducted by several researchers [20, 64-66] provided the insights of dislocation-twin boundary interaction mechanisms of various nanotwinned FCC samples. In order to describe the dislocation-TBs reactions, the Thomson tetrahedron (Figure 1.13 (a, b)) notation could be used.

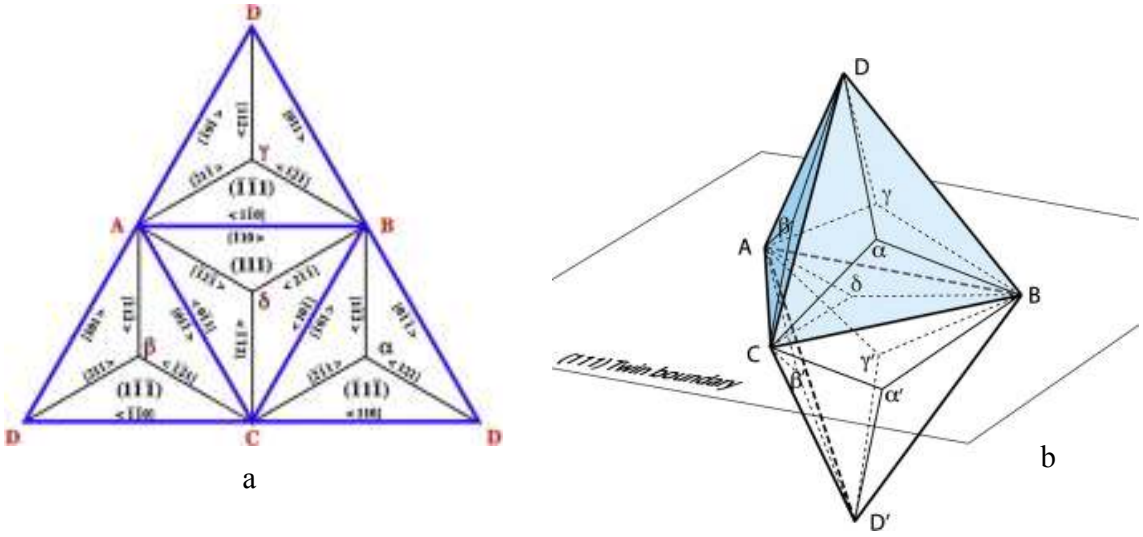

Figure 1. 13 Thompson tetrahedron (a) Two-dimensional representation illustrating the possible slip planes and the Burgers vectors of dislocations in an FCC crystal; (b) Double Thompson tetrahedron [64].

Before the dislocation reacts at a TB, it first glides on a slip plane and stops on a TB, the dislocation line becomes parallel to the intersection between the slip plane and the TB. Consequently, in FCC metals there are four possible types of dislocations to react with the TB: 30^0 Shockley partial, 90^0 Shockley partial, a screw perfect dislocation, and 60^0 perfect dislocation. Below the description of one possible reaction between dislocation and TB is given for an example. More information regarding the dislocation-TB reactions can be found in the papers [11, 64-66].

30^0 Shockley partial dislocation Bα cross-slips into the twin at TB plane BCD, it can react at the TB to grow the twin, or cause de-twinning if the partial glides in the opposite direction after cross-slip. Using the Thompson tetrahedron notation, the following reaction can be written as

$$B\alpha \rightarrow B\delta + \delta\alpha \qquad [1.4.1]$$

Bα is 30^0 partial dislocation that slips in the BCD plane, δα is a stair-rod dislocation at the TB, Bδ is partial that glides on the TB and either thickens or reduces the twin interior by one atomic plane[64].

An alternative reaction of the 30^0 partial can be illustrated with the double Thompson tetrahedron (Figure 1.13 (b)) that above the (111) TB represents matrix slip systems, while the bottom tetrahedron represents twin slip systems. 30^0 partial can be transmitted across the TB according to the following dislocation reaction

$$B\alpha \rightarrow B\alpha' + \alpha'\alpha \qquad [1.4.2]$$

$B\alpha'$ is a partial that can slip away in the twin from the TB on the BCD' plane, and $\alpha'\alpha$ is a new type of stationary stair-rod dislocation across the TB. The transmission reaction is energetically more plausible than that of the cross-slip [11, 64].

1.5 Thesis objectives

The most important and desirable properties for dynamic conductive metals include both high strength and high electrical conductivity. However, many strengthening mechanisms including grain size refinement produce crystalline imperfections that serve as the scattering centers for electrons in metals and therefore lower the conductivity. The introduction of the coherent TBs, is an effective strategy in increasing strength and have an electron scattering coefficient that is an order of magnitude lower than that of conventional high-angle GBs [11].

In the present study, MD simulation technique has been used to simulate the behavior of a columnar nanotwinned Cu under the application of external loads. In view of previous encouraging experimental and simulation results described in the literature review, the following goals of the present research were identified:

1) To elucidate the deformation behavior and the stress-strain response of nanotwinned Cu structures.
2) To reveal the underlying physics of the twin strengthening phenomenon.
3) To investigate the behavior of nanotwinned systems in the critical size range when the softening may occur.
4) To study the effects of the twin space in the system with a constant twin density on the atomistic deformation processes and the corresponding changes in the observed properties.

Chapter 2 Computational approach

Significant progress has been reached in the experimental studies of the structure and evolution of deformed nanocrystalline materials. However, in many cases, the nanocrystalline structures and deformation mechanisms operating in them cannot be unambiguously identified with the help of contemporary experimental methods, because of high precision demands on experiments at the atomic and nanoscale levels. In these circumstances, the employment of both analytical theoretical models and numerical methods is a must for understanding the fundamental nature of the outstanding mechanical properties of nanocrystalline materials. Finite element methods and molecular dynamics are the two numerical methods used to model nanocrystalline materials [27]. The approach of the finite element method consists of subdividing the sample of interest into a number of discrete domains and by using polynomial functions to approximate the true course of a state function over each sub domain [67]. Therefore, the finite element approach is a continuum modeling method with no intrinsic length scale; it allows performing the simulations of complicated geometries with a rational amount of computational work. However, at the nanoscale, the validity and accuracy of the continuum model is the primary issue since the finite element model requires including the separate specialized models. In contrast, the molecular dynamics (MD) directly models the atoms and therefore directly incorporates the atomic length scales of the crystal directly into the computation. Each atom in MD method, represented as a point mass in space, interacts through forces field defined by potential functions.

The first introduction of the MD method is dated back to the late 1950s and early 1960s by Alder and Wainwright [68] and by Rahman [69] in the studies of the dynamics of liquids. Real materials MD simulation was conducted by Gibson et al. in analyzing copper's radiation damage [70]. Due to the revolutionary advances in computer technology and algorithmic improvements, MD has subsequently become a valuable tool in many areas of physics and chemistry [71]. For date, computer simulations act as a bridge between microscopic length and time scales and the macroscopic world of the laboratory. The number of simulation techniques has greatly expanded; there exist now many specialized techniques for particular problems.

MD simulation has several advantages over experimental investigation, which make it a powerful tool for studying nanocrystalline materials. MD simulation can elucidate the detailed atomic level deformation mechanisms, including twinning and defect evolution and interaction, of the complex nanocrystalline systems that are inaccessible experimentally. It is also capable of deforming samples to very large plastic strains, which make it possible to investigate the deformation behavior under high dislocation densities [11]. Finally, MD simulation is more effective and easy to control computational experiment's conditions such as temperature and pressure when material's size is down to nanometer scale. MD method, however, also has its own limitations. First, it typically allows one to study materials with nano-scale dimension, which brings the discrepancy in direct comparisons to macroscopic experiments. The second limitations of MD simulations is its short time duration [72], which results

in extremely high strain rates (typically larger than 10^7 s^{-1}) that are generally inaccessible experimentally. Since it is well known that the strain rate has significant effect on deformation mechanisms, the issue in MD simulations is whether it can actually capture experimentally observed deformation processes. The third limitation of MD is the maximum time step for which the integration of equation of motion is still stable. A typical value of the time step (2 fs) limits the length of current simulations to the nanosecond time scale, making the simulations prohibitively costly [11]. Consequently, the computational methods available for simulating nanocrystalline materials could be deficient sometimes. At the same time, simulation technique is still capable of providing important insights into the possible structural transformation occurring in nanoscale materials. MD approach is treated to be one of effective methods of nanomaterials science and expected to grow rapidly in the future in parallel with progress in hardware and software of computer simulations [1].

The present chapter will give a comprehensive overview of the simulation methods, algorithms for integrating Newton's equation, potential functions, temperature and pressure control, common neighbor analysis, as well as simulation set up.

2.1 Newton mechanics

Molecular dynamics simulation explores the macroscopic properties of a system through microscopic simulations via statistical mechanics which provides mathematical expressions that relate macroscopic properties to the distribution and motion of the atoms and molecules of the N-body system. MD simulation

consists of the numerical solution of the classical Newton's Second equations of motion, which for a simple atomic system may be written as

$$F_i = m_i \frac{\partial^2 r_i(t)}{\partial t^2} \qquad [2.1.1]$$

where $r_i(t). = (x_i(t), y(t), z_i(t))$ is the position vector of i_{th} particle and F_i is the forces acting on the atom of the mass m_i at time t. To integrate the above second order deferential equations the instantaneous forces acting on the particles and their initial positions and velocities must be specified. The acting force of each atom is derived from the potential energy $U(r^n)$ of N interacting atoms as a function of their positions r_i.

$$F_i = -\nabla U(r_i) \qquad [2.1.2]$$

The accurate choice of potential would directly determine the reliability of simulation results. More information on potential choice will be given in the part 2.3.

Combining the two equations [2.1.1] and [2.1.2] together, we obtain the following differential equation

$$\frac{\partial U}{\partial r} = -\frac{\partial^2 r_i(t)}{\partial t^2} \qquad [2.1.3]$$

As shown earlier, the integration of the equation [2.1.3] of each atom yields the trajectories, i.e. positions, velocities and accelerations of each atom as a function of time. Due to the many-body nature of the problem the equations of motion are discretized and solved numerically. The most widely used method to solve the equations [2.1.1] and [2.1.2] is the velocity-Verlet finite-difference

algorithm which has many desirable properties, and will be described in the next part.

2.2 Molecular Dynamics Algorithm

All the integration algorithms assume the positions, velocities and accelerations can be approximated by a Taylor series expansion. The starting point of this algorithm is the Taylor expansion of the particle coordinates around time *t*

$$r_i(t+\Delta t) = r_i(t) + v_i(t)\Delta t + \frac{a(t)}{2}\Delta t^2 + \theta(\Delta t^4) \qquad [2.2.1]$$

and similarly

$$r_i(t-\Delta t) = r_i(t) - v_i(t)\Delta t + \frac{a(t)}{2}\Delta t^2 + \theta(\Delta t^4) \qquad [2.2.2]$$

After adding [2.2.1] and [2.2.2] together, we get

$$r_i(t+\Delta t) + r_i(t-\Delta t) = 2r_i(t) + a(t)\Delta t^2 + \theta(\Delta t^4) \quad [2.2.3]$$

where $\theta(\Delta t^4)$ is the truncation error term of the equations [2.2.2] and [2.2.3]. After rearranging, we get

$$r_i(t+\Delta t) = 2r_i(t) - r_i(t-\Delta t) + a(t)\Delta t^2 \qquad [2.2.4]$$

At this stage, this equation gives rise to the position Verlet algorithm. The Verlet algorithm uses positions *r* and accelerations *a* at time t and the positions from time $(t+\Delta t)$ to calculate new positions at time $(t+\Delta t)$. The Verlet algorithm uses no explicit velocities; they can be calculated from the positions with the accuracy of $\theta(\Delta t^2)$ as

$$v(t) = \frac{r(t+\Delta t) - r(t-\Delta t)}{2\Delta t} + \theta(\Delta t^2) \qquad [2.2.5]$$

The Verlet algorithm is straightforward, simple to implement, accurate and stable, requiring reasonable storage capacity. The main problem with this version of the Verlet algorithm is that velocities are not directly generated. In practice, however, we may need the velocities to calculate quantities such as the kinetic energy, temperature, and correlation functions involving velocities. It is possible to cast the Verlet algorithm in a form which gives both positions and velocities at a given time

$$r_i(t + \Delta t) = r_i(t) + v_i(t)\Delta t + \frac{a(t)}{2}\Delta t^2 \qquad [2.2.6]$$

$$v_i(t + \Delta t) = v_i(t) + \frac{a(t)+a(t+\Delta t)}{2}\Delta t \qquad [2.2.7]$$

This is known as the velocity-Verlet algorithm, also called the leapfrog method. The accuracy for predicting the calculated velocities is up to $\theta(\Delta t^4)$, which is superior to position Verlet algorithm. First, the new positions at time $(t + \Delta t)$ are calculated from the equation [2.2.6], and the velocities at mid-step are calculated using

$$v_i\left(t + \frac{1}{2}\Delta t\right) = v_i(t) + \frac{1}{2}a(t)\Delta t \qquad [2.2.8]$$

The forces and accelerations at time $(t + \Delta t)$ are then computed, and the velocity move completed

$$v_i(t + \Delta t) = v_i\left(t + \frac{1}{2}\Delta t\right) + \frac{1}{2}a(t + \Delta t)\Delta t \qquad [2.2.9]$$

The exact trajectories correspond to the limit of an infinitely small integration step. It is, however, desirable to use larger time steps to sample longer

trajectories. At the same time, energy conservation degrades if the time step is too large. If it is too large, the calculated trajectory will less accurately follow the true trajectory. Thus, there is a compromise between economy and accuracy. In practice Δt is determined by fast motions in the system. Bonds involving light atoms vibrate with periods of several femtoseconds (10^{-15} s), implying that Δt should be on a subfemtosecond scale to ensure stability of the integration [71].

2.3 Interatomic potential

Potential energy function is used to model the basic interactions between constituent atoms or molecules. The accurate choice of interatomic potential function is necessary in every atomistic simulation since it determines the quality of the simulation results and the amount of computer time required. In the following section the short discussion of the pair potential and many-body potential is given.

2.3.1 Pair-body potential (Lennard-Jones potential)

The pair potential treats the overall energy of the system as a sum of atomic pair wise interactions while many-body potential considers energy contribution from the third and more atoms in addition to the pair wise interaction. Lennard-Jones or otherwise known as 12-6 potential is a classical pair potential shown as

$$U_{LJ} = 4\varepsilon\left[\left(\frac{\sigma}{r}\right)^{12} - \left(\frac{\sigma}{r}\right)^{6}\right] \qquad [2.3.1.1]$$

where the parameters σ is the finite distance at which the inter-particle potential is zero, r is the distance between particles, and ε is the well depth are chosen to fit

the physical properties of the material. The first term $\left(\frac{\sigma}{r}\right)^{12}$ models the repulsion energy between two atoms, and it dominates at short distance, while the second term $\left(\frac{\sigma}{r}\right)^{6}$ dominates at large distances and models the attraction energy. Lennard-Jones potential formula is convenient for simulations due to its simplicity and less required computer sources. At the same time, it is sometimes incapable for accurate description of specific materials properties. For example, it fails to estimate the structure relaxation and reconstruction around point defects in metals. The vacancy formation energy obtained by means of pair-wise potentials is overestimated. However, the importance of Lennard-Jones potential cannot be underestimated since the simulation work done on Lennard-Jones systems helped to understand basic points in many areas of condensed matter physics.

2.3.2 Many-body potential (Embedded Atom Method)

Many-body potential has a higher capability for describing the atomic interactions comparing to the pair-wise potential. Embedded Atom Method (EAM) potential is one of the most developed and tested potential type in numerous simulations. Derived in 80's by Daw and Baskes[73], EAM method is based on density functional theory to calculate ground-state properties of realistic metal system. Each atom is viewed as an embedded impurity in the host consisting of all other atoms. Consequently, the EAM includes two terms: pair interactions between nuclei of atoms *i* and *j*, while the second part incorporates the embedding energy as a function of the local background electron density around *i*.

$$U_{tot} = \sum_i F_i\,(p_j(r_{ij}) + \frac{1}{2}\sum_i \sum_{j\neq i} \varphi_{ij}(r_{ij}) \qquad [2.3.2.1]$$

Here, F_i is the embedding energy function, p_j is the spherically averaged background electron density due to the neighbors of the i_{th} atom, φ_{ij} is the pair interaction and r_{ij} is the separation distance between atoms i and j. The embedding energy F_i is assumed to depend only on the local background electron density p_j provided by the surrounding atoms and its lower derivatives.

$$p_j(r_{ij}) = \sum_{j\neq i} p_j(r_{ij}) \qquad [2.3.2.2]$$

In theory, the summations of i and j is performed over all the N atoms. However in practice, j denotes only the neighboring atoms within specified cutoff distance, r_{cut}, of atom i. This cutoff distance typically includes 12 nearest neighbor for perfect FCC and HCP crystals, 14 nearest neighbors for perfect BCC crystals; beyond these neighbors atomic interaction is neglected [74]. The EAM is applicable for examining systems with crystalline defects as grain boundaries or dislocations due to the local background electron density. The present thesis used the Mishin *et al.* form of EAM potential for copper [75] that was developed more recently to fit additional structural properties, such as the stacking fault energy.

2.4 Ensembles

2.4.1 Temperature control (NVT)

Standard molecular dynamics scheme, based on the time integration of Newton's equations, usually leads to the conservation of the total energy. These simulations are performed in the microcanonical ensemble (NVE) ensemble that represents the collection of all states with fixed number of atoms, volume of the

systems and total energy. However, it is often more desirable to perform simulations in the canonical (NVT) ensemble or isothermal-isobaric (NPT) ensemble. To keep the temperature constant, the simulated system can be brought into thermal contact with a large heat bath. One way of mimicking the thermalizing effect of a heat bath is called the Andersen thermostat [76]. The velocity at random intervals of a randomly selected particle is replaced by a new vector, chosen at random from a Maxwell-Boltzmann distribution. The method mimics collision with an imaginary, thermally equilibrated particle. Alternative to the Andersen thermostat, one might use the extended system methods. The idea behind this approach is to extend the system by adding into the simulation extra degrees of freedom that correspond to the heat bath. As a result, one can perform deterministic MD simulations at constant temperature. One such method is known as the Nose-Hoover thermostat proposed by Nose [77] and Hoover [78]. The coupling breaks the energy conservation that otherwise restricts the behavior of the system and leads to the generation of a canonical ensemble. In a method, this is achieved by introducing a time-dependent frictional term, whose time evolution is driven by the imbalance between the instantaneous kinetic energy and the average kinetic energy $(3N/2)k_BT$. The conservation of energy still holds in the composite system, but the total energy of the simulated system is allowed to fluctuate [79].

Velocity-scaling method is another approach for mimicking the effect of a heat bath. This method was employed in the present thesis. The relationship between the temperature and the kinetic energy of the system can be written as

$$T = \frac{2K}{k_B(3N-N_c)} \quad [2.4.1.1]$$

where k_B is Boltzmann constant, N_c is the constraint degree of freedom, $(3N - N_c)$ denotes the total degrees of freedom of the 3D atomistic model with the total N atoms. As so, if the temperature of the system increases, kinetic energy should also increase.

At each time step, the magnitude of the velocity $\overline{V_i}$(t) of each atom is multiplied by a scale factor λ as follows

$$\bar{V}_{i,scaled} = \lambda \overline{V_i}(t) \quad [2.4.1.2]$$

$$\lambda = \left(\frac{T_{req}}{\tau}\right)^{1/2} \quad [2.4.1.3]$$

where τ is the current kinetic temperature, and T_{req} is the desired thermodynamics temperature. The variation of temperature ΔT can be presented as

$$\Delta T = T_{req} - T(t) = (\lambda^2 - 1)T(t) \quad [2.4.1.4]$$

As a result, if the temperature *T(t)* is higher than the prescribed T_{req}, then the system will reduce in velocity, or reduce the kinetic energy. As such, the system temperature will be reduced. Conversely, if the kinetic energy is increased, the temperature will increase [80].

2.4.2 Pressure control (NPH)

In this thesis study, uniaxial tensile test was performed by changing a periodic dimension in size due to constant box deformation. Every 100th time step during the run, we apply true stress and the simulation box expands. To control

the pressure the isobaric- isoenthalpic NPH ensemble that maintains constant enthalpy H and constant pressure P applied was chosen. This ensemble is commonly used in molecular simulations. Developed by H. C. Andersen in 1980 [81], the general approach of the ensemble is to introduce additional degree of freedom to the system, which represents the dynamical variable volume V of a system which is coupled to particle coordinates. Newton's equations of motion are solved for the extended system involving both particle coordinates and volume. The NPH ensemble could be extended to generate the more useful NPT ensemble via a stochastic process. The NPT ensemble has the best approximation for the experimental conditions. To perform molecular dynamics calculations in the NPT ensemble, a number of methods have been developed over the last twenty years using the extended system methodology, including algorithms by Andersen (1980), Parrinello and Rahman (1981). Each of these methods allows the periodic system cell to change its size, driven by the imbalance between the internal and desired system pressures or stresses. In general, constant pressure algorithms have a close analogy to constant temperature algorithms, as an isobaric 'friction' coefficient is introduced to couple the system pressure or stress to an external reservoir.

Suppose the simulation cell has N particles with an arbitrary shape described by three vectors *a,b*, and *c*. h is the matrix formed by {a,b,c} and the volume is

$$\Omega = ||h|| = a \cdot (b \wedge c) \qquad [2.4.2.1]$$

In order to describe the atoms positions of the simulation cell in the shape and size, besides the usual set of 3N dynamical variables, variability is augmented by the nine components of h. Thus, the Hamiltonian is expressed as

$$H = \sum_i \frac{1}{2} m_i v_i^2 + \sum_i \sum_{j>i} \varphi(r_{ij}) + \frac{1}{2} WTr\dot{h}\dot{h} + p\Omega \qquad [2.4.2.2]$$

where the first two terms are kinetic and potential energy functions respectively, **W** is the mass with dimensions and *p* is the pressure. According to the equation, the shape of the simulation cell is allowed to vary and NPH ensemble is generated.

2.5 Periodic boundary conditions

As mentioned earlier, one of the inherent limitations of MD methods is the intrinsic length scale. The size of the simulated systems is limited by the computational resources, and the number of atoms in the system would be always negligible compared with the numbers of atoms in a bulk material. The use of periodic boundary conditions (PBC) is a solution to this problem. Figure 2.1 illustrates a schematic representation of periodic boundary condition in the atomistic framework.

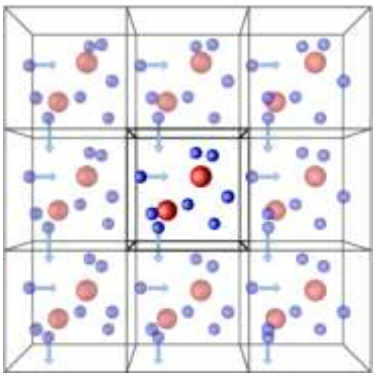

Figure 2. 1 Schematic representations of periodic boundary conditions.

Atoms that lie within the primary cell in the center are explicitly modeled using atomistic methods. The bordering cells, that are also called “image” cells, represent the infinite replication of the primary cell. As a result, an infinite amount of material is modeled in each direction. During the simulation, as an atom moves to the point outside of the primary cell, one of its images will enter through the opposite side with the same momentum. Atoms lying near the boundaries interact with the neighboring atoms residing within the cutoff radius across the boundaries. This interaction permits the atoms near the surfaces to see their full neighbors similar to the atoms inside the bulk and is required for accurate force and energy calculation. Hence, the physical behaviors and properties of the primary cell can represent the corresponding macroscopic sample of interest.

Each unit cells represented may contain a defect. The use of PBC introduces interactions between a number of dislocations. This interaction, will, to some extent, affect the atomic and electronic structure, especially if the number of atoms in the cell is small [82].

2.6 Atomic strain tensor

Modeling the mechanical behavior of nanostructures, it is necessary to compute a map of the stress distribution over the individual atomic sites in a system composed of N atoms.[83]. LAMMPS simulations provide the symmetric per-atom stress tensor at the end of each time step that has 6 components, stored in the following order: xx, yy, zz, xy, xz, yz. The stress tensor contains one normal σ and two shear τ components (Figure 2.2). The commonly known Virial

theorem is used to evaluate these stresses for atom *I* [61] by the following formula:

$$S_{ab} = -\left[mv_a v_b + \frac{1}{2}\sum_{n=1}^{N_p}(r_{1a}F_{1b} + r_{2a}F_{2b})\right] \qquad [2.6.1]$$

where *a* and *b* take on values x, y, z to generate the 6 components of the symmetric tensor. The first term is a kinetic energy contribution for atom *I*, with m and v denoting its atomic mass, and the velocity of atom *I*, respectively. The second term is a pair-wise energy contribution where *n* loops over the N_p neighbors of atom *I*, r_1 and r_2 are the positions of the 2 atoms in the pair-wise interaction, and $F_1$and F_2 are the forces on the 2 atoms resulting from the pair-wise interaction.

In the present studies, we have calculated the stress mapping to characterize the mechanical response of nanotwinned copper under tension in order to find out the sites of stress concentration where the dislocation nucleation is most probable. The principal stress value is used to provide a clear view of stress state system [84].

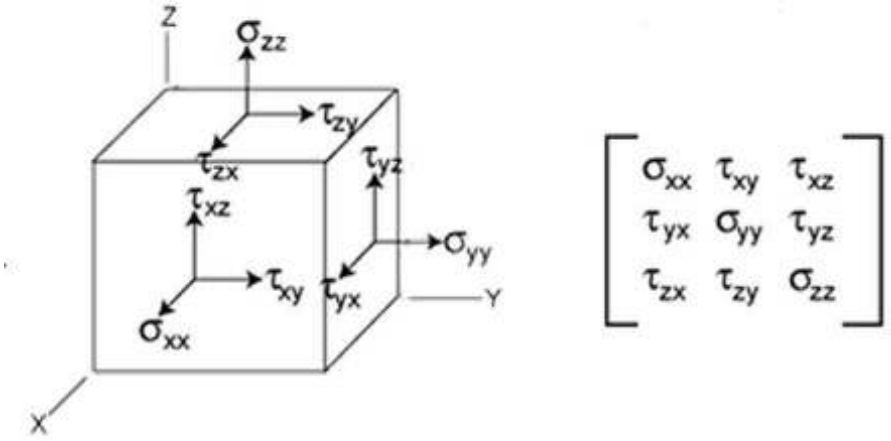

Figure 2. 2 Stress tensor in three dimensions.

In order to determine the principal stress of the stress tensor, the basis should be changed in such a way that the shear stress components become zero. In this case, the stress tensor is represented by a diagonal matrix

$$\sigma_{ij} = \begin{pmatrix} \sigma_1 & 0 & 0 \\ 0 & \sigma_2 & 0 \\ 0 & 0 & \sigma_3 \end{pmatrix} \qquad [2.6.2]$$

The components of the stress tensor depend on the orientation of the coordinate system at the point under consideration. However, the stress tensor itself is a physical quantity and as such, it is independent of the coordinate system chosen to represent it. There are certain invariants I_1, I_2, I_3 of stress tensor, always with the same value regardless of the coordinate system's orientation. One set of such invariants are the principal stresses, which are the eigenvalues of the stress tensor. They can be found from the determinant equation

$$\begin{vmatrix} \sigma_{xx} - \lambda & \tau_{xy} & \tau_{xz} \\ \tau_{yx} & \sigma_{yy} - \lambda & \tau_{yz} \\ \tau_{zx} & \tau_{zy} & \sigma_{zz} - \lambda \end{vmatrix} = 0 \qquad [2.6.3]$$

Expanding the determinant leads to the cubic characteristic equation from which the three real roots λ can be found as

$$\lambda^3 - I_1\lambda^2 + I_2\lambda - I_3 = 0 \qquad [2.6.4]$$

where

$$I_1 = \sigma_1 + \sigma_2 + \sigma_3$$

$$I_2 = \sigma_1\sigma_2 + \sigma_2\sigma_3 + \sigma_1\sigma_2 \qquad [2.6.5]$$

$$I_3 = \sigma_1\sigma_2\sigma_3$$

The principal stresses $\sigma_1, \sigma_2, \sigma_3$, functions of the eigenvalues λ_i, can be found as

$$\sigma_1 = \max(\lambda_1, \lambda_2, \lambda_3)$$

$$\sigma_3 = \min(\lambda_1, \lambda_2, \lambda_3) \qquad [2.6.6]$$

$$\sigma_2 = I_1 - \lambda_1 - \lambda_3$$

2.7 Common neighbor analysis (CNA)

During the tensile test the lattice defects are introduced. Thus, the underlying deformation mechanisms could be investigated by filtering out the uninteresting atoms that are not associated with the defects directly. In order to identify the location and character of the nucleated defects, and visualize the nucleation and evolution process of the defects common neighbor analysis (CNA) [85] [86] was used. This method analyzed the neighbors of each atom, and recognized the crystalline structures such as FCC or BCC, HCP. As a result, one can distinguish atoms that belong to the defects such as grains, grain boundaries, stacking faults and vacancies.

CNA method performs a geometric analysis [87] of the first shell of nearest neighbors around a reference atom. A cut-off radius represents the distance between the reference atom and one of its nearest neighbors. It is usual specified by the primary crystal structure and the lattice constant of the material under consideration. Atoms closer to each other than the given threshold radius are connected by an edge in the abstract graph. The common neighbor analysis uses the topological nearest-neighbor information of this mathematical graph structure to determine the crystalline arrangement around each atom. Each crystal structure exhibits a characteristic local topology of the nearest-neighbor graph. The cutoff radius if the face-centered cubic (FCC) and hexagonal close packed (HCP) structures is lied midway between the first and the second shell of neighbor atoms. The following formula can be used to obtain a good cutoff distance in LAMMPS MD code for FCC materials:

$$r_c^{fcc} = \frac{1}{2}\left(\frac{\sqrt{2}}{2} + 1\right) a \simeq 0.8536a \qquad [2.7.1]$$

where *a* is the lattice constant for the crystal structure concerned.

Since the CNA calculation in LAMMPS uses the neighbors of an owned atom to find the nearest neighbors of a ghost atom, the following relation should also be satisfied:

$$R_c + R_s > 2 * cutoff \qquad [2.7.2]$$

where *Rc* is the cutoff distance of the potential, *Rs* is the skin distance as specified by the neighbor command.

The introduced method has a simple interpretation with the manageable number of types of features, and it is powerful to clearly distinguish between various local structures [88].

2.8 Simulation set-up

2.8.1 Model description

In order to analyze the deformation behavior and responses of the nanotwinned structure in the tensile test, a computation model has been built using a series of computer programs written in C programming language. The simulation cell with a <011> columnar textured microstructure contains four hexagonal grains of face-center-cubic (FCC) copper with lattice constant 3.615 Å. The grains are equiaxed and separated by narrow grain boundaries. Figure 2.1 depicts grain 1 oriented with the crystallographic directions [111], [$\bar{1}\bar{1}2$] and [110] in the X-, Y- and Z-directions, respectively (Figure 2.3). The misorientation angles for the other three grains rotated around [110] tilt axis are chosen as 40^0, -40^0, and -90^0. According to "Mackenzie plot" [89, 90], that shows the disorientation angle distribution for equiaxed grains in cubic crystals, the highest population of the GBs is found for the misorientation angle around 40^0. The large angle of the grain boundary was also chosen due to the fact that small angle grain boundaries are weak obstacles to the plastic flow when compared to large angle grain boundaries because they can be penetrated by dislocations which continue their glide path in the neighboring crystal [91].

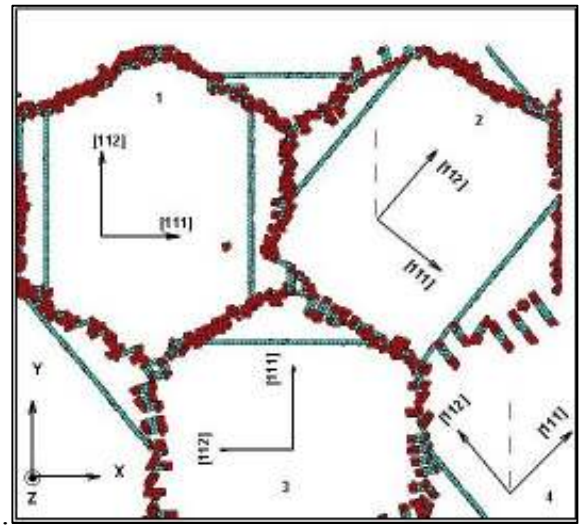

Figure 2. 3 Initial configuration of the periodic computational cell with four hexagonal grains with embedded nanotwins.

The columnar simulation geometry of the model limits all dislocation lines to be parallel to the [011] columnar z-axis, and following their nucleation dislocations can glide only on any of the two active {111} <112> slip systems in each grain. The systems with a grain of 7.5 nm and 15 nm have dimensions of 15 nm×13 nm×3.8 nm and 30 nm×26 nm×3.8 nm which contains about 62903 and 251610 atoms, respectively. An embedded-atom method (EAM) potential developed by Mishin et.al [92] is used in the present studies to describe the many-body interactions among atoms. For comparison, we looked at different nanotwinned models by varying the twin spacing between 1.25 and 6.27 nm for the smaller grain and between 1.25 and 12.5 nm for the bigger one, but keeping the density of twins always constant.

For the purpose of analyzing the deformation mechanisms and viewing defects in the samples, colors are assigned to the atoms according to the common

neighbor analysis (CNA). 3 types of atoms are painted in color: blue stands for FCC atoms, light blue for HCP atoms (stacking faults and twin boundaries), red for unknown atoms that might represent dislocations, vacancies and grain boundaries. Intrinsic stacking faults appear as two adjacent (111) planes of HCP atoms, while extrinsic stacking faults are two (111) planes of HCP atoms separated by a single (111) plane of FCC atoms. A single line of HCP atoms represents a TB.

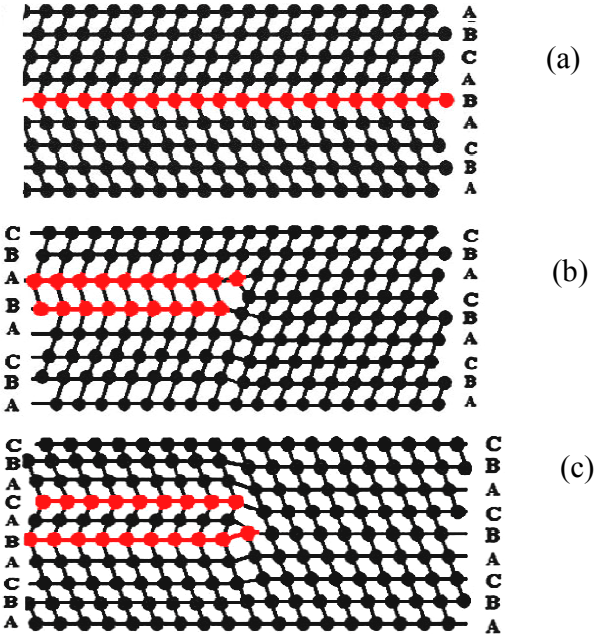

Figure 2. 4 Stacking faults identified by CNA. (a) Twin boundary. (b) An intrinsic stacking fault. (c) An extrinsic stacking fault.

2.8.2 System relaxation

Molecular Dynamics simulations are performed via "Large-scale Atomic/Molecular Massively Parallel Simulator" LAMMPS from Sandia National Laboratories. Before applying the tensile loading, the initial nanotwinned

structure is relaxed under both zero bar pressure and constant temperature of 900 K for 200 ps, and then gradually cooled down to the room temperature of 300K. The relaxation runs at NPH ensemble, where the temperature was controlled by using the rescaling method mentioned above.

2.8.3 System deformation

At the beginning of each simulation and before applying the tensile deformation, a Gaussian distribution of the velocities of all the atoms is generated using a random number generator at a specific temperature. After equilibration process, we applied constant true strain rate of $3*10^7$ s^{-1}, which allows the structure to deform up to 15% of strain in the x-direction. The simulations are performed in constant NPH ensemble. Periodic boundary conditions were imposed in all directions. Atomic positions, velocities, and accelerations are updated at each time step using the Velocity-Verlet algorithm. The total simulation time is set at 5000 ps with a time step of 0.002 ps. The temperature of the simulations controlled using a rescaling method is set for 300K. Due to the large volume of data generated in each time step, only atom id and type, as well as the atomic coordinates are stored every 20ps for post-processing.

Chapter 3. Simulation results and discussion

The results of the computational tensile tests performed for different nanotwinned models are presented below. First, the corresponding stress vs. strain curves for systems with and without nano twins are compared and examined. Secondly, the observed deformation behaviors are discussed. After, the effect of twin width (λ) and grain size (d) on mechanical properties is investigated. Finally, the results and conclusions are summarized.

3.1 Stress-strain response variation of the nanotwinned models

The dependence of the mechanical behavior of the nanostructured Cu on the strain rate of the tensile tests is of a great importance. The usual response for the increase in strain rate of a material for which dislocation slip is dominant deformation mechanisms is increase in tensile strength. The materials with a predominant deformation twinning mode show decrease in flow stress and tensile strength when the loading rate increases [93]. Figure 3.1 summarizes the stress-strain curves for nanocrystalline twinned Cu at different tensile strain rate. As shown, the yield strength and tensile strength increase with increasing loading rate. For the present simulation we chose high strain rate of 3×10^{7} s^{-1}, which allows the structure to deform up to 15%. Such a high rate is unrealistic in a physical sense, but inherent to every MD simulation since it is necessary to obtain a significant amount of deformation within a reasonable time.

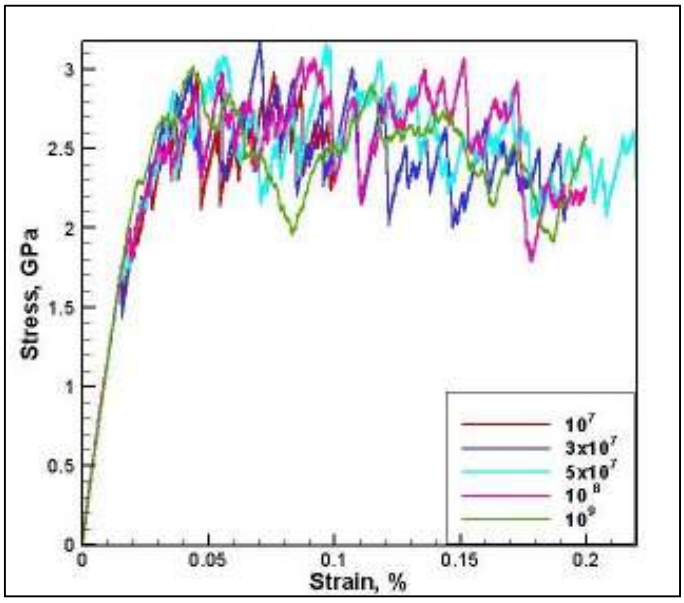

Figure 3. 1 Stress-strain curves for NC Cu at different strain rates (s^{-1}).

Typical tensile stress-strain curves for system with and without growth twins are shown in Figure 3.2.

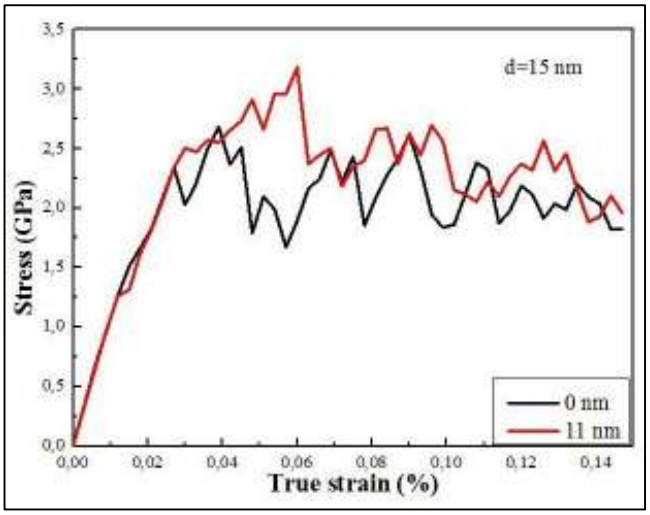

Figure 3. 2 Comparison between simulated stress-strain (σ-ε) curves for grain size samples of 15 nm with and without twins under uniaxial tensile loading strain rate of 3×10^7 s^{-1} and 300 K temperature.

As illustrated, both systems exhibit initial elastic behavior, followed by the occurrence of yielding, corresponding to the emission of first partial dislocations from the GBs. Later, for the nanotwinned model dislocations start to accumulate against the TBs, and as a result, the system reaches higher stress, comparing to the twin-free models, where the dislocation motion is not restricted. Afterwards, the stress values gradually decrease with increasing strain when the slip transfer occurs across the TBs. Since the plasticity of nanocrystalline material is determined via the emission of first individual dislocation from GBs and triple junctions, the corresponding yield strength of the nanotwinned and twin-free samples is almost comparable. The elastic modules of twin-free and twinned systems are~ 97.56 GPa and 106 GPa, respectively. The stress required to cause plastic deformation, or flow stress, in the present research was calculated by averaging the instantaneous stress value from 5 to 11% strain. The results show that flow stress increases from 2.21 to 2.49 GPa for twin-free and samples with coherent twin. Upon tensile loading, the twinned sample shows pronounced elevated strength than that of twin-free system while possessing a considerable tensile elongation up to 15%. The unique combination of two properties such as strength and ductility is due to the pinning effect of TBs on dislocation motion during plastic deformation, and TB-mediated mechanisms operating on the latter stages that contribute to tensile ductility.

To understand possible sources for dislocation nucleation in nano-twinned metals, we have determined the distribution of the principle stress σ_1 (GPa) before yielding in three different twin-space models as shown in Figure 3.3.

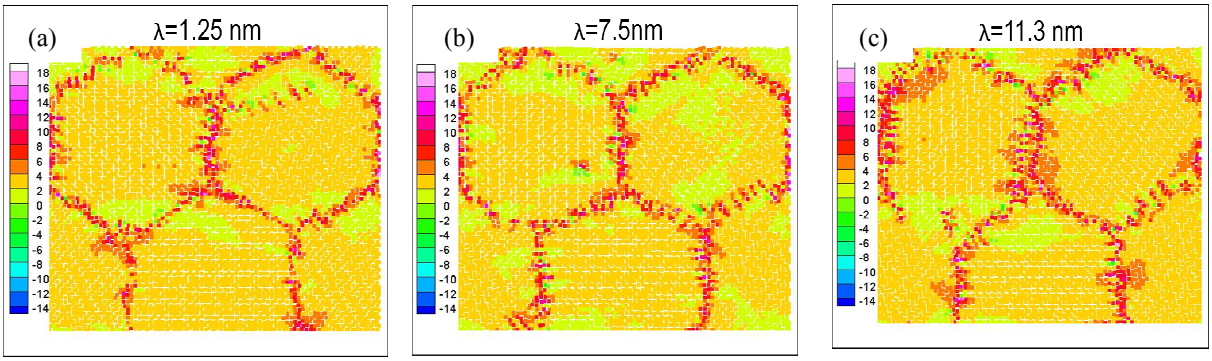

Figure 3. 3 Distribution of principal stress in different twin spacing systems before yielding: (a) 1.25 nm corresponding to GB/TB distance of 6.87 nm), (b) 7.5 nm corresponding to GB/TB distance of 3.75 nm and (c) 11 nm corresponding to GB/TB distance of 2 nm.

The colored atoms reflect the local stress magnitude, and from the color bar red color stands for higher stress than the green one. According to the map, stress concentration is clearly seen at GBs and triple junctions. High stress concentration is attributed to the disordered structure of the GBs. As s result, interfacial imperfections of the GBs act as preferential regions of dislocation emission when the external stress is applied.

3.2 Deformation behavior

Several mechanisms have been identified during process of plastic deformation. Figure 3.3 shows the snapshots of deformation activities inside the grain of twin-free sample at the strain of 2.5% and 5%.

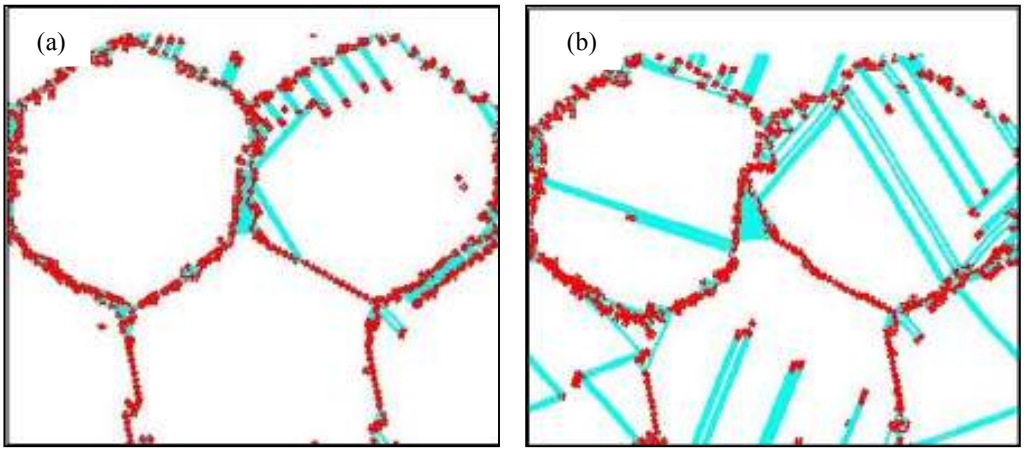

Figure 3. 4 Snapshots of uniaxial tensile deformation of twin-free sample at 2.5% (a) and 5% (b) strain rate.

It is seen, that upon the tensile loading, the leading Shockley partial dislocations of 1/6[112] nucleate from the GB or triple junction (Figure 3.4(a)), sweep across the nanosized grain, experiencing no obstacles on their way, and eventually annihilate at the opposite GB interface. At this stage, the trailing partials were not emitted from the GBs, which is in the agreement with the previous researches [10, 94, 95]. As a result, an intrinsic stacking fault, typically longer than the equilibrium spacing between partial dislocations, remained within the grain (Figure 3.4(b)). The dislocation activity within the grains is the predominant mechanism of plastic deformation of twin-free samples.

A dynamic observation of the dislocation evolution during the initiation and propagation of plastic deformation of the nano-twinned sample with twin lamella of 5 nm is shown in Figure 3.5.

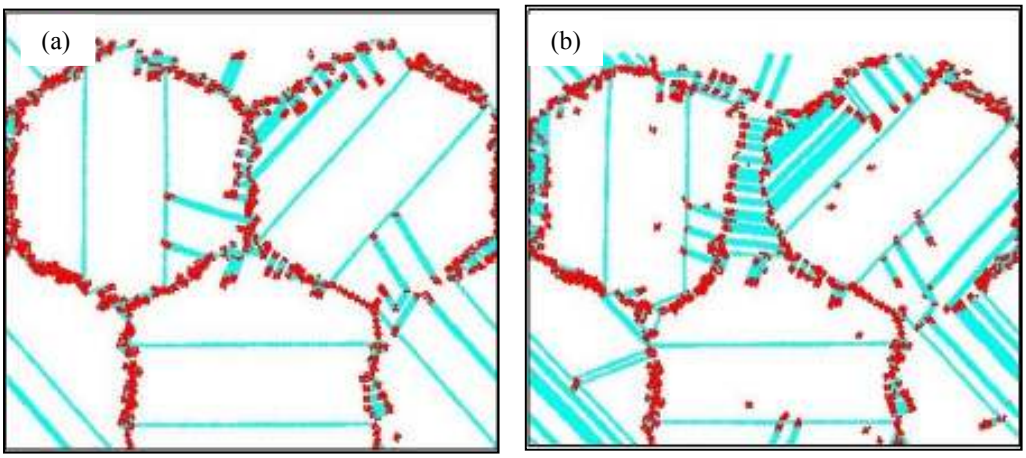

Figure 3. 5 Snapshots of uniaxial tensile deformation of nanotwinned sample (λ=5nm) at 2.5% (a) and 5% (b).

Nanotwinned copper exhibits a very heterogeneous deformation behavior. Depending on the local GB and TB orientation, we observed a combination of the following deformation mechanisms: emission of partial dislocations from the GBs, intrinsic stacking fault formation, TB migration and deformation twinning. There are two sets of slip planes in our samples: one runs parallel to the TBs, while the other intersects the TB at an angle of 70^0. The nucleation of partial dislocations begins from the GBs and triple junctions (Figure 3.5 (a)). The emitted partial dislocations with the Burgers vector of the 1/6{111}<112> type move through the grains gliding along two slip systems and leaving behind an intrinsic stacking faults. In some cases (grain 2, Figure 3.5 (b)) after a leading partial dislocation is emitted, the nucleation of the trailing partial on the same slip plane that creates a full dislocation was observed. The possibility of trailing partial nucleation on the same slip plane is controlled by the ratio $\frac{\gamma_{sf}}{\gamma_{utf}}$ [10]. For Cu this

energy ratio is 0.13, that is far from unity. Despite this fact, the slip via full dislocation on the same slip plane was still detected.

The deformation mode depends on the orientation of each individual grain boundary relative to the loading axis. Critical resolved shear stress or Schmid factor that is the component of shear stress, resolved in the direction of slip, necessary to initiate slip in a grain, was calculated. Table 1 presents the calculated Schmid factor of two planes in each grain along and across the TBs.

	Grain 1	**Grain 2**	**Grain 3**	**Grain 4**
Slip 1	0	0.492	0.203	0.485
Slip 2	0.203	0.485	0	0.492

Table 1. 1 Schmid factor for different grains.

As expected, the majority of dislocation accumulation occurs on slip plane with high Schmid factors. Comparable Schmid factors of the grains 2 and 4 promote the dislocation glide to occur along and across the TBs. While grain 1 experiences major deformation on transverse glide planes, and TBs act as obstacles and have a strengthening effect, grain 3 shows a maximum Schmid factor at the plane parallel to TBs, when the dislocation glide is not blocked and contribute to the overall ductility of the material. The variations of Schmid factor in different grains ultimately dictate the deformation behavior in each grain. Based on the above discussion, it can be said that the elevated strength of the nanotwinned models is attributed mostly to the deformation behaviors in grains 1, 2 and 4, while the contribution to the ductility of materials is due to the grain 3.

The motion of the leading partial dislocations is hindered by the TBs, resulting in a dislocation accumulation across the TBs (Figure 3.5(b)). These dislocations with the stacking faults bridging TBs and GBs, inhibit the nucleation and motion of other dislocations, contributing to the strength of the material. As the stress increases, the energy barrier of the twins can be overcome, and these trapped dislocations can react with the TBs, resulting in cross-slip, formation of sessile stair-rod dislocation or transmission across the TB. The snapshots in Figure 3.6 depict the possible dislocation reactions at the TB at 10% strain rate.

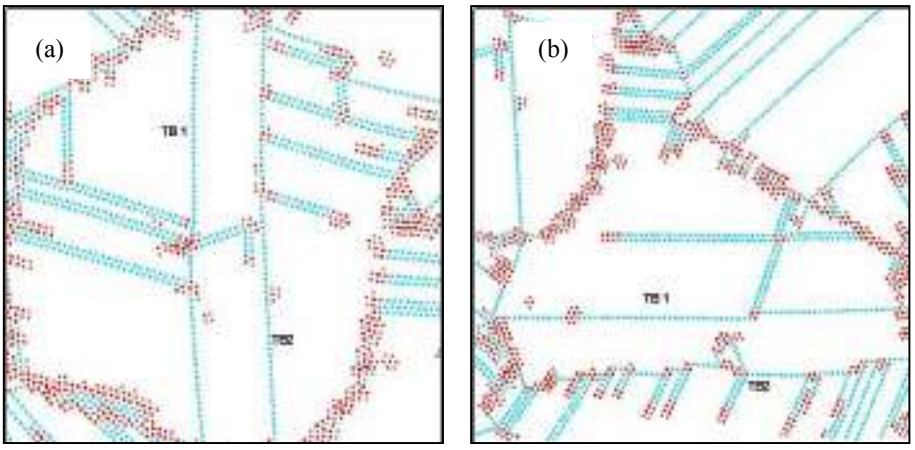

Figure 3. 6 The nucleation and propagation of dislocations from TBs in grain 1 (a) and grain 3 (b) at 10% strain rate.

The transmission motion of the dislocation across the TB for the grain 1 is illustrated in Figure 3.6 (a). Such dislocation structure has been observed in the previous simulations as well [95-97]. As an extended dislocation approaches to the first TB_1, its 1/6[121] leading partial is first blocked where it meets the TB. With the increase of the stress, this TB-blocked dislocation disassociates into two partials: Shockley 1/6[211] dislocation that propagates into the twinned crystal,

leaving behind an intrinsic stacking fault and a stationary Frank partial that remains in the TB_1 plane. Newly generated Shockley partial on several different slip systems contributes to the ductility of the material, while the formation of Frank partial dislocations could lead to the ultrahigh strength. This scenario is energetically plausible since the energy barrier small enough for the partial dislocation to be transmitted across the TB. Previous investigations have reached the same conclusions [95-97]. Figure 3.6(b) demonstrates the cross-slip of the leading partial dislocation onto the TB_2 plane and the consequent formation of a stair-rod dislocation. Later, one partial dislocation that leaves behind the step on the TB_2, glides to the left and move the TB towards the interior by one atomic plane. Stair-rod dislocation could further dissociate into two partial causing the de-twinning process [64].

The simulation has also revealed the nucleation of deformation twins from GBs. After a leading partial dislocation is emitted, the heterogeneous nucleation of the twins takes place by emission from the GB of successive 1/6[112] edge partials on adjacent (111) planes. These twinning partials moving through the grain on adjacent crystal planes create an extrinsic stacking fault. Two coherent twin boundaries are separated later by two (111) planes, and in the end they turned to more widely separated twins [62]. Successive emissions of partials on the adjacent slip planes widen the thickness of the twinning fault. The possibility of creating a new partial in the neighboring slip plane is defined by the ratio $\frac{\gamma_{utf}}{\gamma_{usf}}$.

From the above experimental observations, one can clearly see that the mechanical properties of nanocrystalline materials are controlled by their unique

deformation mechanisms. The presence of nanoscale TBs in nanocrystalline copper provides an effective approach for simultaneous improvement of the strength and the ductility of the material.

3.3 Twin spacing variation

3.3.1 Effect on strength

As mentioned earlier, the presence of nanoscale TBs in Cu provides adequate barriers to dislocation motion for strengthening, as well as significantly increases the dislocation storage capability in materials. At a smaller twin-boundary thickness (Figure 3.7(a)), when the TBs are located rather far from the GBs, a large number of partial dislocations nucleate in multiple slip systems and then assemble together in the pile-up at the TBs. Dislocations accumulated across the TBs propagate across the twins, undergoing dislocation dissociation reactions, which require stress concentrations at twin-slip band intersection. As a result, a pronounced stress concentration at the TBs is produced, leading to the lower applied stress required to activate the slip transmission across the TBs. If the TBs are far enough from each other (Figure 3.7(b)), partial dislocations emitted from the GBs have shorter free paths before they encounter the TBs. Thus, the dislocation propagation and interaction is constricted, and less of them are accumulated at the TBs. In this case an extremely high stress is required for the following deformation process.

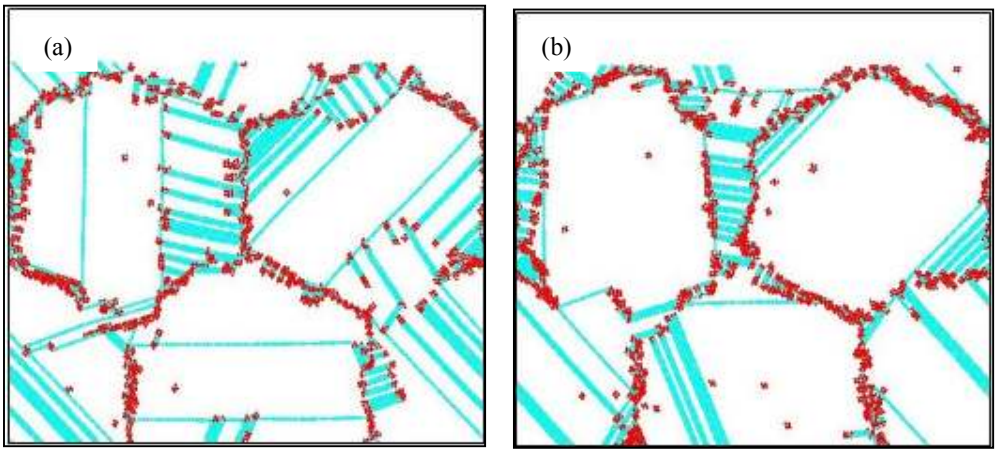

Figure 3. 7 Deformation snapshots of dislocation emission from the TBs at the same strain 0.05 for the two systems: (a) of 5 nm twin spacing, (b) of 11 nm.

In order to calculate the stress required to produce plastic deformation, we calculated the flow stress. Figure 3.8 depicts a variation of the average flow stress for the grain size of 15 nm as a function of twin spacing. As shown, a maximum strength of the material is achieved at a minimal TB/GB distance that corresponds to the twin spacing of 11 nm. Subsequent decrease in the distance between TBs and GBs down to 1.25 nm that corresponds to the twin thickness of 12.5 nm, results in a significant decrease in strength.

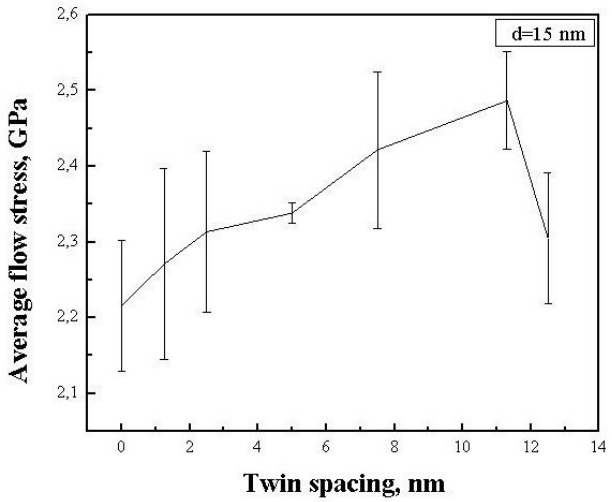

Figure 3. 8 Averaged flow stress from a strain of 5-11% for d =15 nm versus twin spacing.

Lu et al. [51] suggested that the strongest twin thickness originates from a transition in the yielding mechanism from the slip transfer across twin boundaries to the activity of preexisting easy dislocation sources. However, the observed strength softening in our simulations cannot be caused by pre-existing dislocations because of the initially dislocation-free samples.

The maximum strength was further investigated using large-scale MD simulations and a kinetic theory of dislocation nucleation by Li et al. [52]. The proposed dislocation–nucleation-controlled mechanism in nano-twinned metals suggests that dislocation nucleation governs the strength of materials, resulting in the softening of the materials below a critical twin thickness. They found that there exists a transition in deformation mechanism, occurring at a critical twin-boundary spacing for which strength is maximized. At this point, the classical Hall–Petch type of strengthening due to dislocation pile-up and cutting through

twin planes switches to a dislocation–nucleation-controlled softening mechanism with twin-boundary migration resulting from nucleation and motion of partial dislocations parallel to the twin planes.

To elucidate the observed softening we compared the deformation patterns of the samples with different twin spacing at the same deformation strain 12.5% (Figure 3.9). As illustrated, the dislocation configurations vary with the thickness of twin lamellae. For samples with a TB spacing of 12.5 nm (Figure 3.9 (a)) at the later stages of deformation, when the dislocation density nucleated from the GBs is high, we observed considerable twinning fault formation. Our simulation revealed different mechanisms for nucleation of microtwins, including the emission of extrinsic stacking faults from the GBs, stacking-fault overlapping or partial-dislocation breakaway. In this case, the contribution of twinning partials to the flow stress and work hardening is pronounced and leads to their reduction.

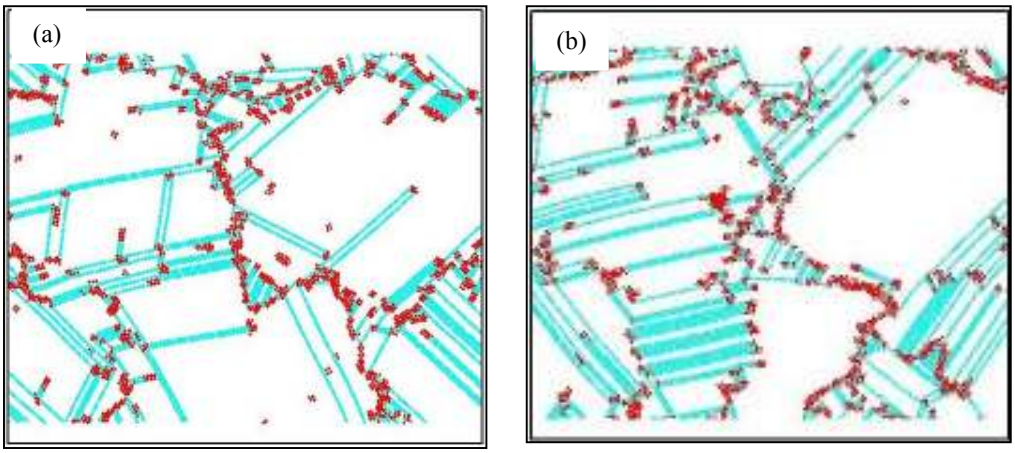

Figure 3. 9 Deformation snapshots of dislocation emission from the TBs at the same strain 0.12 for the three systems: (a) of 12.5 nm twin spacing, (b) 11 nm.

In contrast, for the samples with 11 nm twin spacing (Figure 3.9(b)) we revealed a large amount of dislocation debris in the vicinity of TBs, as well as the formation of Lomer-Cottrell locks in each of the four grains. The density of twinning partials is not significant, therefore the observed dislocation accumulation in the samples is considered responsible for the work hardening in the tensile stress-strain curve.

3.3.2 Effect on toughness

It is known that nanotwinned samples experience the unique behavior exhibiting both enhanced strength and ductility with decreasing TB/GB spacing. The controlled loading of our simulation doesn't lead to the abrupt, catastrophic failure of a purely uniaxial test. Thus, we select a measure of toughness to as the energy absorption capability of the material that is usually determined by both the strength and the ductility. Its calculation helps to quantify the effects of adding nanotwins on both properties of the samples. The toughness value of Cu with nanotwins was calculated by summing up the areas under the global normal stress versus strain curves. The values are plotted against the twin width for 15 and 7.5 nm grain size models (Figure 3.10).

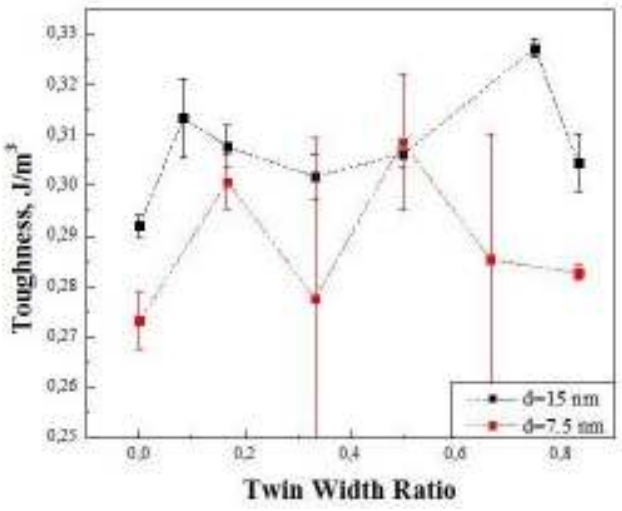

Figure 3. 10 The toughness variation with twin width for from a strain of 5-11% for d =15 nm and 7.5 nm.

The figure implies that for both grain sizes the twinned models exhibit higher toughness than the twin-free model and the toughness considerably increases for the nanotwinned model with decreasing TB/GB distance and increasing twin spacing. The observed trend is in a good agreement with the previous simulation results [95, 98] and experiments [7, 8]. The observed high toughness could be attributed to the confinement effect of dislocation motion by the TBs. The dislocation movement across and along the TBs is affected by the twin spacing. When the TBs are close enough to the GBs, the dislocation propagation path is short due to the presence of twins that block the dislocation movement effectively with a low degree of dislocation emission. The confinement of dislocation results in a decreased toughness.

As the grain size is reduced to 7.5 nm, toughness value is decreased for all nanotwinned systems due to the decrease in ductility. Free dislocation movement

of the dislocation in the grain interior promotes high ductility in the material. Therefore, the larger grain models have longer free dislocation paths, and consequently exhibit higher toughness value. It is important to notice that as the system size decreases, the uncertainty of toughness increases, as demonstrated by the larger data scattering. Further studies are needed in order to clarify this issue in the extremely small nano-crystal size.

3.4. Effect of twin spacing and grain refinement

In this last section we examine both grain size and twin space refinement, and try to evaluate how to refine both these to parameters to optimize the strength and toughness.

One of the other possible ways for the optimized combination of high strength and high ductility metals is the grain refinement of the nanotwinned structure. Grain refinement is a conventional way of the strengthening, which is usually described by the well-known Hall-Petch effect. However, the enhancement in strength usually leads to the significant reduction in ductility. In contrast, nanotwinned structures exhibit an increase in both strength and ductility with twin width refinement. Experimental research and atomistic simulations on many nanocrystalline materials demonstrate a strength softening mechanism for grain sizes below 10 nm, which has been attributed to a transition from dislocation-mediated plastic deformation to GB-associated mechanism such as GB sliding and rotation. In the present simulation study, we investigated the effect of grain size and twin spacing refinement on the flow stress by determining the

flow stress of nanotwinned Cu as a function of TB spacing at different grain size ranging from 15 down to 7.5 nm (Figure 3.11).

An inverse Hall-Petch effect was observed for the grain size ranging from 15 to 7.5 nm. The figure shows that the critical twin spacing that corresponds to the maximum flow strength depends on the grain size: for the smaller grain size, the maximum strength corresponds to the twin boundary spacing of 5 nm (GB/TB distance is 1.25 nm), while for the bigger grain size twin spacing is 7.5 nm (GB/TB distance is 3.75 nm). This result agrees well with the previous MD simulations of strengthening in nanotwinned copper [52, 99].

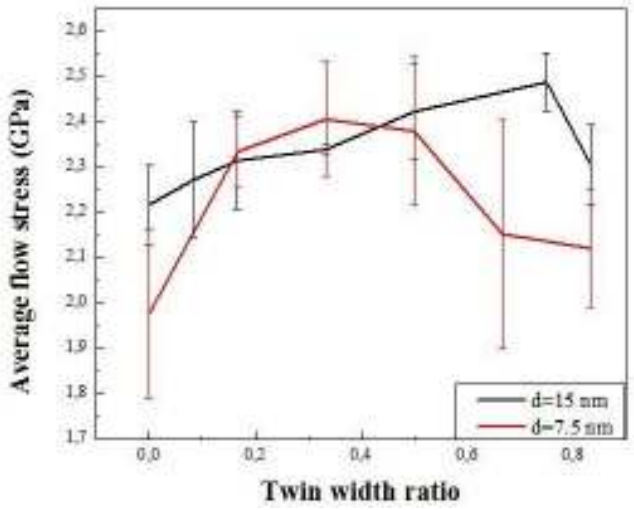

Figure 3. 11 Flow stress of nano-twinned Cu as a function of twin width ratio at different grain size.

In order to find out the cause of the inverse Hall-Petch relation occurrence, we tracked the relative displacement of the center of mass between two neighboring grains. This displacement helps to quantify the sliding of the GBs. A certain amount of atoms that are far away from the GBs are selected to calculate

the grain mass. The displacement between two mass centers is illustrated in Figure 3.12. It is evident from the figure that the movement of the grains 1 and 2 move relative to each other for the grain size system of 7.5 nm is more pronounced than for the bigger grain size. Thus, the obtained results show the presence of GB sliding resulting in the inverse Hall-Petch relation.

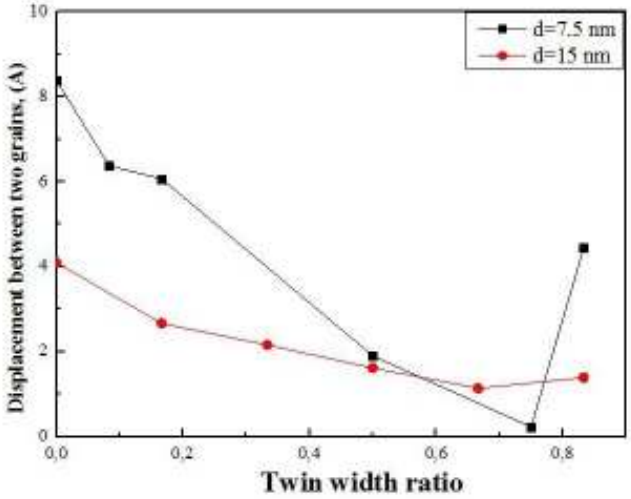

Figure 3. 12 Grain boundary displacement vs. twin spacing for the system with different grain size at 10% strain.

3.5 Summary

In the present research we have examined the deformation mechanisms of columnar-grained nanocrystalline materials under tensile loading for the systems with different twin boundary spacing but fixed density of TBs. The results have shown that:

1) Nanotwinned Cu exhibits the unique combination of high strength and ductility, due to effect of TBs on dislocation motion during plastic deformation,

and TB-mediated mechanisms operating on the latter stages that contribute to tensile ductility.

2) GB-mediated deformation mechanisms of nanotwinned Cu has been identified as the dominant in the present simulation. The deformation mode depends on the orientation of each individual grain boundary relative to the loading axis.

3) Nanotwinned Cu exhibits the increase in strength, hardness and toughness with the refinement of TB/GB distance. Maximum strength of the material is achieved at a TB/GB distance of 2 nm that corresponds of to the twin spacing of 11 nm. Subsequent decrease in the distance between TBs and GBs results in softening of the material.

4) The correlated properties of high strength, high toughness and strong work hardening in nanotwinned metals are sensitive to both twin spacing and grain size refinement. The optimization strategy is in terms of reducing the TB spacing and the grain size as much as feasible.

Chapter 4 Conclusion and future work

4.1 General conclusions

The potential applications of nanotechnology are immense. Particularly, nanotwinned copper is considered as the main candidate for conducting material due to combination of substantial mechanical strength, good ductility and high electrical conductivity. In the present research, we aimed to develop a complete understanding of the underlying deformation mechanisms that govern the observed macroscopic properties of nanotwinned Cu. We used molecular dynamics simulation methods to study the mechanical response of nanotwinned Cu under uniaxial tensile loading condition. For comparison, different nanotwinned models at different grain size (15 and 7.5 nm) were constructed by varying twin spacing and keeping the twin boundary density constant. The stress-strain responses of various models were compared. The effect of twin spacing and grain size on the microscopic deformation behavior and properties was examined. The following conclusions can be made:

1) In tensile test, nanotwinned Cu exhibits significantly improved mechanical properties as compared to twin-free samples. The combination of high strength and ductility is attributed to the coherent nanoscale twin boundaries. During the plastic deformation, nanoscale twins impart strength to the material due to dislocation motion restriction, and simultaneously contribute to the tensile ductility on latter stages of deformation due to TB-mediated mechanisms. Opposed

to TBs, Grain boundaries usually posses highly disordered structure, and are found to be the most probable sites for dislocation nucleation.

2) GB-mediated deformation mechanisms of nanotwinned Cu has been identified as the dominant in the present simulation. It includes extended and partial dislocation emission from the GBs; interaction of the partials with the TBs; twinning fault formation; dislocation emission from the TBs; GB sliding. The deformation mode depends on the orientation of each individual grain boundary relative to the loading axis. For example, grains 2 and 4 with the orientation at 40^0 and -90^0 to the loading axis show comparable deformation across and along the TBs, whereas grain 3 oriented at -40^0 exhibit deformations mostly at the plane parallel to the TBs. Therefore, the grain orientations should be taken into consideration in order to optimize nanotwinned materials' properties.

3) The increase in strength, hardness and toughness in nanotwinned Cu happen with the refinement of TB/GB distance that is comparable with the increase in twin spacing. Maximum strength of the material is achieved at a TB/GB distance of 2 nm that corresponds to the twin spacing of 11 nm. Subsequent decrease in the distance between TBs and GBs results in softening of the material. We concluded that the dislocation configurations varying with the thickness of twin lamellae is responsible for the observed strength impairment. In particular, abundant nucleation of twinning partials dislocations governs the

softening in nano-twinned metals when the twin spacing reaches 11 nm.

4) The correlated properties of high strength, high toughness and strong work hardening in nanotwinned metals are sensitive to both twin spacing and grain size refinement. Grain size refinement results in an increase in strength and decrease in ductility. Inverse Hall-Petch relation was observed when the grain size of the model is below 7.5 nm. The simulation results suggest that the inverse Hall-Petch relation result from the GB sliding.

4.2 Future work

The present study can be extended in many possible ways in order to get further insight of the nanotwinned structures. Some of them are suggested below:

1) The present work deals with a specific GBs misorientation angle. In order to improve the understanding of the GBs and TBs influence on deformation mechanisms of nanocrystalline copper, different boundary orientation can be used.
2) The simulation model investigated in the present research is exclusively columnar, based on the periodic boundary conditions. Such geometry limits dislocation glide to happen only on two active slip planes. In addition, the limited number of grains in a periodic cell imposes constraints on the plasticity of the model. To get a more realistic picture it is thus important to extend this present work into a 3-dimensional model set up consists of a large number of randomly

oriented grains. This would give an opportunity to compare the results with experimental observations.

3) As mentioned, nanotwinned Cu as a candidate of electrical contacts requires having superior mechanical properties combines with low electrical resistivity. The contribution of the twin spacing and grain size to the electrical resistivity variation when the plastic deformation occurs needs to be investigated in-depth studies in the future.

The proposed strategies will help to enhance the understanding of the unique characteristics of the nanotwinned structures and also will clarify the potential engineering applications of this new class of material.

Bibliography

[1] C. C. Koch, *Structural Nanocrystalline Materials: Fundamentals and Applications.* Cambridge: Cambridge University Press, 2007.

[2] Y. Wang, M. Chen, F. Zhou and E. Ma, "High tensile ductility in a nanostructured metal," *Nature,* vol. 419, pp. 912-915, 2002.

[3] L. Lu, Y. Shen, X. Chen, L. Qian and K. Lu, "Ultrahigh Strength and High Electrical Conductivity in Copper," *Science,* vol. 304, pp. 422-426, 04/16, 2004.

[4] E. Ma, "Strain hardening and large tensile elongation in ultrahigh-strength nano-twinned copper," *Appl. Phys. Lett.,* vol. 85, pp. 4932-3, 2004-11-23T15:30:44, 2004.

[5] O. Anderoglu, "Epitaxial nanotwinned Cu films with high strength and high conductivity," *Appl. Phys. Lett.,* vol. 93, pp. 083108-3, 2008-08-26T13:15:48, 2008.

[6] I. Nakamichi, "Electrical resistivity and grain boundaries in metals," *Materials Science Forum,* vol. 207-209, pp. 47-58, 1996.

[7] M. Dao, L. Lu, Y. F. Shen and S. Suresh, "Strength, strain-rate sensitivity and ductility of copper with nanoscale twins," *Acta Materialia,* vol. 54, pp. 5421-5432, 12, 2006.

[8] Y. F. Shen, L. Lu, Q. H. Lu, Z. H. Jin and K. Lu, "Tensile properties of copper with nano-scale twins," *Scr. Mater.,* vol. 52, pp. 989-994, 5, 2005.

[9] T. Zhu, J. Li, A. Samanta, H. G. Kim and S. Suresh, "Interfacial plasticity governs strain rate sensitivity and ductility in nanostructured metals," *Proceedings of the National Academy of Sciences,* vol. 104, pp. 3031-3036, February 27, 2007.

[10] H. Van Swygenhoven, P. M. Derlet and A. G. Froseth, "Stacking fault energies and slip in nanocrystalline metals," *Nat Mater,* vol. 3, pp. 399-403, print, 2004.

[11] Y. T. Zhu, X. Z. Liao and X. L. Wu, "Deformation twinning in nanocrystalline materials," *Progress in Materials Science,* vol. 57, pp. 1-62, 1, 2012.

[12] X. Liao, "Deformation twinning in nanocrystalline copper at room temperature and low strain rate," *Appl. Phys. Lett.,* vol. 84, pp. 592-3, 2004-01-21T09:02:59, 2004.

[13] M. Dao, L. Lu, R. J. Asaro, J. T. M. De Hosson and E. Ma, "Toward a quantitative understanding of mechanical behavior of nanocrystalline metals," *Acta Materialia,* vol. 55, pp. 4041-4065, 7, 2007.

[14] J. Schiotz and K. W. Jacobsen, "A Maximum in the Strength of Nanocrystalline Copper," *Science,* vol. 301, pp. 1357-1359, 09/05, 2003.

[15] A. H. Chokshi, A. Rosen, J. Karch and H. Gleiter, "On the validity of the hall-petch relationship in nanocrystalline materials," *Scripta Metallurgica,* vol. 23, pp. 1679-1683, 10, 1989.

[16] H. Van Swygenhoven, A. Caro and D. Farkas, "A molecular dynamics study of polycrystalline fcc metals at the nanoscale: grain boundary structure and its influence on plastic deformation," *Materials Science and Engineering: A,* vol. 309-310, pp. 440-444, 7/15, 2001.

[17] V. Yamakov, D. Wolf, S. R. Phillpot, A. K. Mukherjee and H. Gleiter, "Deformation-mechanism map for nanocrystalline metals by molecular-dynamics simulation," *Nature Materials,* vol. 3, pp. 43-47, 2004.

[18] J. Schiøtz, F. D. Di Tolla and K. W. Jacobsen, "Softening of nanocrystalline metals at very small grain sizes," *Nature,* vol. 391, pp. 561-563, 1998.

[19] V. Yamakov, D. Wolf, S. R. Phillpot and H. Gleiter, "Dislocation–dislocation and dislocation–twin reactions in nanocrystalline Al by molecular dynamics simulation," *Acta Materialia,* vol. 51, pp. 4135-4147, 8/15, 2003.

[20] V. Yamakov, D. Wolf, S. R. Phillpot, A. K. Mukherjee and H. Gleiter, "Dislocation processes in the deformation of nanocrystalline aluminium by molecular-dynamics simulation," *Nature Materials,* vol. 1, pp. 45-48, 2002.

[21] C. C. Koch, "Ductility in nanostructured and ultra fine-grained materials: Recent evidence for optimism," *Journal of Metastable and Nanocrystalline Materials,* vol. 18, pp. 9-20, 2003.

[22] C. Koch, K. Youssef, R. Scattergood and K. Murty, "Breakthroughs in optimization of mechanical properties of nanostructured metals and alloys RID B-9101-2008 RID F-4629-2010 RID D-5204-2009," *Adv. Eng. Mater.,* vol. 7, pp. 787-794, SEP, 2005.

[23] L. Lu, M. Dao, T. Zhu and J. Li, "Size dependence of rate-controlling deformation mechanisms in nanotwinned copper," *Scr. Mater.,* vol. 60, pp. 1062-1066, 6, 2009.

[24] V. L. Tellkamp, A. Melmed and E. J. Lavernia, "Mechanical behavior and microstructure of a thermally stable bulk nanostructured Al alloy," *Metall Mat Trans A Phys Metall Mat Sci,* vol. 32, pp. 2335-2343, 2001.

[25] D. Witkin, Z. Lee, R. Rodriguez, S. Nutt and E. Lavernia, "Al–Mg alloy engineered with bimodal grain size for high strength and increased ductility," *Scr. Mater.,* vol. 49, pp. 297-302, 8, 2003.

[26] A. V. Sergueeva, N. A. Mara and A. K. Mukherjee, "Grain size distribution effect on mechanical behavior of nanocrystalline materials," in *Materials Research Society Symposium Proceedings,* 2004, pp. 243-249.

[27] M. A. Meyers, A. Mishra and D. J. Benson, "Mechanical properties of nanocrystalline materials," *Progress in Materials Science,* vol. 51, pp. 427-556, 5, 2006.

[28] H. Van Swygenhoven and P. M. Derlet, "Grain-boundary sliding in nanocrystalline fcc metals," *Physical Review B - Condensed Matter and Materials Physics,* vol. 64, pp. 2241051-2241059, 2001.

[29] A. Hasnaoui, H. Van Swygenhoven and P. M. Derlet, "Cooperative processes during plastic deformation in nanocrystalline fcc metals: A molecular dynamics simulation," *Physical Review B - Condensed Matter and Materials Physics,* vol. 66, pp. 1841121-1841128, 2002.

[30] A. V. Sergueeva, N. A. Mara, N. A. Krasilnikov, R. Z. Valiev, A. K. Mukherjee, "Cooperative grain boundary sliding in nanocrystalline materials," *Philos Mag,* vol. 86, pp. 5797, 2006.

[31] N. Q. Chinh, P. Szommer, Z. Horita and T. G. Langdon, "Experimental evidence for grain-boundary sliding in ultrafine-grained aluminum processed by severe plastic deformation," *Adv Mater,* vol. 18, pp. 34-39, 2006.

[32] I. A. Ovid'ko and A. G. Sheinerman, "Enhanced ductility of nanomaterials through optimization of grain boundary sliding and diffusion processes," *Acta Materialia,* vol. 57, pp. 2217-2228, 200904, 2009.

[33] A. P. Sutton and R. W. Balluffi, Ed., *Interfaces in Crystalline Materials.* 1996.

[34] H. Conrad and J. Narayan, "On the grain size softening in nanocrystalline materials," *Scr. Mater.,* vol. 42, 2000.

[35] H. Conrad and J. Narayan, "On the grain size softening in nanocrystalline materials," *Scr. Mater.,* vol. 42, pp. 1025-1030, 2000.

[36] M. Ke, S. A. Hackney, W. W. Milligan and E. C. Aifantis, "Observation and measurement of grain rotation and plastic strain in nanostructured metal thin films," *Nanostructured Materials,* vol. 5, pp. 689-697, 1995.

[37] A. Hasnaoui, H. Van Swygenhoven and P. M. Derlet, "Cooperative processes during plastic deformation in nanocrystalline fcc metals: A molecular dynamics simulation," *Physical Review B - Condensed Matter and Materials Physics,* vol. 66, pp. 1841121-1841128, 2002.

[38] D. Farkas, S. Mohanty and J. Monk, "Strain-driven grain boundary motion in nanocrystalline materials," *Materials Science and Engineering A,* vol. 493, pp. 33-40, 2008.

[39] M. Murayama, J. M. Howe, H. Hidaka and S. Takaki, "Atomic-level observation of disclination dipoles in mechanically milled, nanocrystalline Fe," *Science,* vol. 295, pp. 2433-2435, 2002.

[40] D. Jia, Y. M. Wang, K. T. Ramesh, E. Ma, Y. T. Zhu and R. Z. Valiev, "Deformation behavior and plastic instabilities of ultrafine-grained titanium," *Appl. Phys. Lett.,* vol. 79, pp. 611-613, 2001.

[41] Y. M. Wang, E. Ma and M. W. Chen, "Enhanced tensile ductility and toughness in nanostructured Cu," *Appl. Phys. Lett.,* vol. 80, pp. 2395-2397, 2002.

[42] X. Jianq and C. L. Jia, "The coalescence of [001] diamond grains heteroepitaxially grown on (001) silicon," *Appl. Phys. Lett.,* vol. 69, pp. 3902-3904, 1996.

[43] V. Yamakov, D. Wolf, M. Salazar, S. R. Phillpot and H. Gleiter, "Length-scale effects in the nucleation of extended dislocations in nanocrystalline Al by molecular-dynamics simulation," *Acta Materialia,* vol. 49, pp. 2713-2722, 8/16, 2001.

[44] K. S. Kumar, S. Suresh, M. F. Chisholm, J. A. Horton and P. Wang, "Deformation of electrodeposited nanocrystalline nickel," *Acta Materialia,* vol. 51, pp. 387-405, 1/22, 2003.

[45] X. Z. Liao, "Deformation twins in nanocrystalline Al ," *Appl. Phys. Lett.,* vol. 83, pp. 5062, 2003.

[46] H. Van Swygenhoven, M. Spaczer and A. Caro, "Microscopic description of plasticity in computer generated metallic nanophase samples: a comparison between Cu and Ni," *Acta Materialia,* vol. 47, pp. 3117-3126, 8/10, 1999.

[47] H. Van Swygenhoven, "Atomic mechanism for dislocation emission from nanosized grain boundaries," *Phys. Rev.,* vol. B 66, pp. 024101, 2002.

[48] Hirth, J. P. Lothe, J., *Theory of Dislocations.* New York: John Wiley and Sons Inc, 1991.

[49] S. Jakob, "Atomic-scale modeling of plastic deformation of nanocrystalline copper," *Scr. Mater.,* vol. 51, pp. 837-841, 10, 2004.

[50] M. W. Chen, J. W. McCauley and Dandekar, D. P. Bourne, N. K. Dynamic plasticity and failure of high-purity alumina under shock loading. *Nat Mater 5*pp. 614. 2006/08.

[51] L. Lu, X. Chen, X. Huang and K. Lu, "Revealing the Maximum Strength in Nanotwinned Copper," *Science,* vol. 323, pp. 607-610, January 30, 2009.

[52] X. Li, Y. Wei, L. Lu, K. Lu and H. Gao, "Dislocation nucleation governed softening and maximum strength in nano-twinned metals," *Nature,* vol. 464, pp. 877-880, 04/08, 2010.

[53] K. Lu, L. Lu and S. Suresh, "Strengthening Materials by Engineering Coherent Internal Boundaries at the Nanoscale," *Science,* vol. 324, pp. 349-352, 04/17, 2009.

[54] T. H. Blewitt, R. R. Coltman and J. K. Redman, "Low-temperature deformation of copper single crystals," *J. Appl. Phys.,* vol. 28, pp. 651-660, 1957.

[55] Nolder R. L., *The Substructure of Plastically Deformed Nickel.* 1964.

[56] O. Johari, Ed., *Substructures in Explosively Deformed Cu and Cu-Al Alloys.* 1964.

[57] M. Chen, E. Ma, K. J. Hemker, H. Sheng, Y. Wang and X. Cheng, "Deformation Twinning in Nanocrystalline Aluminum," *Science,* vol. 300, pp. 1275-1277, May 23, 2003.

[58] V. Yamakov, D. Wolf, S. R. Phillpot and H. Gleiter, "Deformation twinning in nanocrystalline Al by molecular-dynamics simulation," *Acta Materialia,* vol. 50, pp. 5005-5020, 12/3, 2002.

[59] D. Wolf, V. Yamakov, S. R. Phillpot, A. Mukherjee and H. Gleiter, "Deformation of nanocrystalline materials by molecular-dynamics simulation: Relationship to experiments?" *Acta Materialia,* vol. 53, pp. 1-40, 2005.

[60] B. Q. Li, M. L. Sui and S. X. Mao, "Twinnability Predication for fcc Metals," *Journal of Materials Science & Technology,* vol. 27, pp. 97-100, 2, 2011.

[61] Ishraq Shabib, "Understanding the mechanical properties of nanotwiined copper using molecular dynamics simulation," 2009.

[62] V. Yamakov, D. Wolf, S. R. Phillpot and H. Gleiter, "Deformation twinning in nanocrystalline Al by molecular-dynamics simulation," *Acta Materialia,* vol. 50, pp. 5005-5020, 12/3, 2002.

[63] Y. T. Zhu, X. L. Wu, X. Z. Liao, J. Narayan, S. N. Mathaudhu and L. J. Kecsḱs, "Twinning partial multiplication at grain boundary in nanocrystalline fcc metals," *Appl. Phys. Lett.,* vol. 95, 2009.

[64] Y. T. Zhu, X. L. Wu, X. Z. Liao, J. Narayan, L. J. Kecskés and S. N. Mathaudhu, "Dislocation–twin interactions in nanocrystalline fcc metals," *Acta Materialia,* vol. 59, pp. 812-821, 1, 2011.

[65] Z. X. Wu, Y. W. Zhang and D. J. Srolovitz, "Dislocation–twin interaction mechanisms for ultrahigh strength and ductility in nanotwinned metals," *Acta Materialia,* vol. 57, pp. 4508-4518, 9, 2009.

[66] Z. -. Jin, P. Gumbsch, K. Albe, E. Ma, K. Lu, H. Gleiter and H. Hahn, "Interactions between non-screw lattice dislocations and coherent twin boundaries in face-centered cubic metals," *Acta Materialia,* vol. 56, pp. 1126-1135, 3, 2008.

[67] K. G. F. Janssens, Ed., *Computational Materials Engineering.* Burlington, MA: Elsevier Academic Press, 2007.

[68] Alder, B. J. , Wainwright, T. E. J., Ed., *Chem. Phys.* 1957.

[69] A. Rahman, "Phys. Rev." *Phys. Rev.,* vol. A136, pp. 405, 1964.

[70] Gibson, J. B., Goland, A. N., Milgram, M. & Vineyard, G. H., Ed., *Dynamics of Radiation Damage.* 1960.

[71] Petrenko, Roman, and Meller, Jarosław. Molecular dynamics. *ELS. John Wiley & Sons Ltd* Mar 2010. Available: [doi: 10.1002/9780470015902.a0003048.pub2];.

[72] D. Wolf, V. Yamakov, S. R. Phillpot, A. Mukherjee and H. Gleiter, "Deformation of nanocrystalline materials by molecular-dynamics simulation: Relationship to experiments?" *Acta Materialia,* vol. 53, pp. 1-40, 2005.

[73] Daw M.S. and Baskes M.I., *Phys. Rev Lett.,* vol. 29:6443, 1984.

[74] Ronald E. Miller., "On the generalization of continuum models to include atomistic features. " 1998.

[75] Y. Mishin, M. J. Mehl, D. A. Papaconstantopoulos, A. F. Voter and J. D. Kress, "Structural stability and lattice defects in copper: Ab initio, tight-binding, and embedded-atom calculations," *Physical Review B - Condensed Matter and Materials Physics,* vol. 63, pp. 2241061-22410616, 2001.

[76] H.C. Andersen, "," *J. Chem. Phys.,* vol. 72, 1980.

[77] S. Nose, *Molec. Phys.,* vol. 52, pp. 255, 1984.

[78] W. G. Hoover, *Phys. Rev.,* vol. A 31, pp. 1695, 1985.

[79] G. A. Mansoori, *Principles of Nanotechnology: Molecular-Based Study of Condensed Matter in Small Systems.* Hackensack, N.J.: World Scientific, 2005.

[80] J. Fan, *Multiscale Analysis of Deformation and Failure of Materials.* Chichester, West Sussex, U.K.: Wiley, 2011.

[81] H. Andersen, "Molecular dynamics simulations at constant pressure and/or temperature," *J. Chem. Phys.,* vol. 72, pp. 2384-2393, 1980.

[82] N. Itoh and A. M. Stoneham, *Materials Modification by Electronic Excitation.* Cambridge, UK ; New York, NY: Cambridge University Press, 2001.

[83] H.Rafii-Tabar G.A. Mansoori, "Interatomic potential models for nanostructures," *Encyclopedia of Nanoscience and Nanotechnology,* .

[84] Lei Yue , "A molecular dynamics modeling study on the mechanical behavior of nanotwinned Cu and relevant issues ," 2010, 2010.

[85] J. D. Honeycutt and H. C. Andersen, "Molecular dynamics study of melting and freezing of small Lennard-Jones clusters," *J. Phys. Chem.,* vol. 91, pp. 4950-4963, 09/10; 2011/11, 1987.

[86] D. Faken and H. Jónsson, "Systematic analysis of local atomic structure combined with 3D computer graphics," *Computational Materials Science,* vol. 2, pp. 279-286, 3, 1994.

[87] T. K. Norbert Lümmen and, "Common neighbour analysis for binary atomic systems," *Modell Simul Mater Sci Eng,* vol. 15, pp. 319, 2007.

[88] D. Faken and H. Jonsson, "Systematic analysis of local atomic structure combined with 3D computer graphics," *Computational Materials Science,* vol. 2, pp. 279-286, 03, 1994.

[89] V. Randle, H. Davies and I. Cross, "Grain boundary misorientation distributions," *Current Opinion in Solid State and Materials Science,* vol. 5, pp. 3-8, 1, 2001.

[90] J. K. Mackenzie, "The distribution of rotation axes in a random aggregate of cubic crystals," *Acta Metallurgica,* vol. 12, pp. 223-225, 1964.

[91] S. Zaefferer, J. -. Kuo, Z. Zhao, M. Winning and D. Raabe, "On the influence of the grain boundary misorientation on the plastic deformation of aluminum bicrystals," *Acta Materialia,* vol. 51, pp. 4719-4735, 9/15, 2003.

[92] Y. Mishin, M. J. Mehl, D. A. Papaconstantopoulos, A. F. Voter and J. D. Kress, "Structural stability and lattice defects in copper: Ab initio, tight-binding, and embedded-atom calculations," *Physical Review B - Condensed Matter and Materials Physics,* vol. 63, pp. 2241061-22410616, 2001.

[93] L. Lu, S. X. Li and K. Lu, "An abnormal strain rate effect on tensile behavior in nanocrystalline copper," *Scr. Mater.,* vol. 45, pp. 1163-1169, 11/19, 2001.

[94] I. Shabib and R. E. Miller, "Deformation characteristics and stress–strain response of nanotwinned copper via molecular dynamics simulation," *Acta Materialia,* vol. 57, pp. 4364-4373, 9, 2009.

[95] A. J. Cao and Y. G. Wei, "Molecular dynamics simulation of plastic deformation of nanotwinned copper," *J. Appl. Phys.,* vol. 102, pp. 083511-5, 2007-10-17T16:13:44, 2007.

[96] Z. X. Wu, Y. W. Zhang and D. J. Srolovitz, "Dislocation–twin interaction mechanisms for ultrahigh strength and ductility in nanotwinned metals," *Acta Materialia,* vol. 57, pp. 4508-4518, 9, 2009.

[97] Y. G. Zheng, J. Lu, H. W. Zhang and Z. Chen, "Strengthening and toughening by interface-mediated slip transfer reaction in nanotwinned copper," *Scr. Mater.,* vol. 60, pp. 508-511, 4, 2009.

[98] A. Frøseth, H. Van Swygenhoven and P. M. Derlet, "The influence of twins on the mechanical properties of nc-Al," *Acta Materialia,* vol. 52, pp. 2259-2268, 5/3, 2004.

[99] L. Zhu, H. Ruan, X. Li, M. Dao, H. Gao and J. Lu, "Modeling grain size dependent optimal twin spacing for achieving ultimate high strength and related high ductility in nanotwinned metals," *Acta Materialia,* vol. 59, pp. 5544-5557, 8, 2011.